Succinate dehydrogenase/complex II is critical for metabolic and epigenetic regulation of T cell proliferation and inflammation

Xuyong Chen[1], Benjamin Sunkel[1], Meng Wang[1], Siwen Kang[1], Tingting Wang[1], JN Rashida Gnanaprakasam[1], Lingling Liu[1], Teresa A. Cassel[2], David A. Scott[3], Ana M. Muñoz-Cabello[4], Jose Lopez-Barneo[4], Jun Yang[5], Andrew N. Lane[2], Gang Xin[6], Benjamin Stanton[1]*****, Teresa W.-M. Fan[2]*****, and Ruoning Wang[1]*****

Affiliations

[1]Center for Childhood Cancer & Blood Diseases, Hematology/Oncology & BMT, Abigail Wexner Research Institute at Nationwide Children's Hospital, The Ohio State University, Columbus, OH, USA.

2Center for Environmental and Systems Biochemistry, Dept. of Toxicology and Cancer Biology, Markey Cancer Center, University of Kentucky, Lexington, KY, USA.

[3]Cancer Metabolism Core, Sanford Burnham Prebys Medical Discovery Institute, La Jolla, CA, USA.

[4]Instituto de Biomedicina de Sevilla (IBiS), Hospital Universitario "Virgen del Rocío"/CSIC/Universidad de Sevilla, Spain.

[5]Department of Surgery, St Jude Children’s Research Hospital, Memphis, TN, USA.

[6]Department of Microbial Infection and Immunity, The Ohio State University, Columbus, OH, USA.

*****Correspondence should be addressed to**:**

Ruoning Wang, Phone: 614-335-2980; Fax: 614-722-5895.

ruoning.wang@nationwidechildrens.org;

Teresa W.-M. Fan, Phone: 858-218-1028, Fax: 859-257-1307.

twmfan@gmail.com;

Benjamin Stanton, Phone: 614-355-2691; Fax: 614-722-5895.

Benjamin.Stanton@nationwidechildrens.org;

One Sentence Summary

The loss of SDH/complex II function blocks cell proliferation but enhances inflammation in T cells.

Abstract

Effective T cell-mediated immune responses require the proper allocation of metabolic resources to sustain growth, proliferation, and cytokine production. Epigenetic control of the genome also governs T cell transcriptome and T cell lineage commitment and maintenance. Cellular metabolic programs interact with epigenetic regulation by providing substrates for covalent modifications of chromatin. By employing complementary genetic, epigenetic, and metabolic approaches, we revealed that tricarboxylic acid (TCA) cycle flux fueled biosynthetic processes while controlling the ratio of succinate/α-ketoglutarate(α-KG) to modulate the activities of dioxygenases that are critical for driving T cell inflammation. In contrast to cancer cells, where succinate dehydrogenase (SDH)/complex II inactivation drives cell transformation and growth, SDH/complex II deficiency in T cells caused proliferation and survival defects when the TCA cycle was truncated, blocking carbon flux to support nucleosides biosynthesis. Replenishing the intracellular nucleoside pool partially relieved the dependence of T cells on SDH/complex II for proliferation and survival. SDH deficiency induced a pro-inflammatory gene signature in T cells and promoted T helper 1 and T helper 17 lineage differentiation. An increasing succinate/α-KG ratio in SDH deficient T cells promoted inflammation by changing the pattern of the transcriptional and chromatin-accessibility signatures and consequentially increasing the expression of the transcription factor, PR domain zinc finger protein 1. Collectively, our studies revealed a role of SDH/complex II in allocating carbon resources for anabolic processes and epigenetic regulation in T cell proliferation and inflammation.

Overline: T cells

T cells need proper fueling

The metabolism of T cells is crucial for proper function, yet many of the metabolic processes involved in various T cell responses are poorly defined. Here, Chen *et al.* used complex analysis of *in vitro* cell culture of mouse T cells to show that succinate dehydrogenase/complex II was crucial for proliferation and inflammatory responses of CD4+ T cells. Knock out or pharmacologic inhibition of this complex led to reduced proliferation and survival, but increased inflammatory responses. Succinate dehydrogenase/complex II deficiency led to altered nucleotide biosynthesis and transcriptional and epigenetic signatures, subsequently increasing B lymphocyte-induced maturation protein-1, a transcription factor crucial for functional T cell activation. Thus, Succinate dehydrogenase/complex II is involved in proper T cell function.

Key Figure: Fig.1I, right

Short title: T cells need succinate dehydrogenase/complex **II**

Introduction

T cell activation engages glycolysis, the pentose phosphate pathway (PPP), and the tricarboxylic acid (TCA) cycle to prepare T cells for growth, differentiation, and immune defense (*1-3*). This conversion is reminiscent of the characteristic metabolic switch during the transformation of normal cells to cancer cells (*4, 5*). In parallel, T cell activation is accompanied by a dynamic remodeling of chromatin accessibility and DNA modifications, which determine the transcriptional status of lineage-specifying genes. Comparative studies reveal epigenetic patterns in accessible, poised, and silenced gene loci in different CD4 subsets (*6-8*). Mapped permissive and repressive epigenetic modifications in lineage-restricting transcription factors and lineage-specific cytokine genes indicate that such a bivalent epigenetic state is critical for T cell lineage commitment (*8-10*). As such, a dynamic epigenetic regulation allows progeny cells to maintain lineage-specific transcription programs while retaining some level of plasticity in response to environmental cues. Also, central carbon metabolism allocates carbon inputs to metabolites that are substrates, antagonists, and cofactors of epigenetic-modifying enzymes. Thus, central carbon metabolism is instrumental in establishing and maintaining the epigenetic landscape for cell fate determination. However, how and which metabolic pathways control the epigenome for the proliferation and differentiation of Teff cells still remains elusive.

While an essential function of the TCA cycle is to sustain the oxidative carbon flux to meet energy consumption needs, the TCA cycle also coordinates the carbon input (anaplerosis) and carbon output (cataplerosis) to ensure biosynthetic activities and epigenetic regulation (*11-13*). Specifically, α-ketoglutarate (α-KG), an intermediate of the TCA cycle, is an essential co-substrate of α-KG dependent dioxygenases such as specific histone and DNA demethylases. In contrast, succinate and fumarate are potent inhibitors of these enzymes (*14*). Therefore, the ratio

changes of these metabolites can impact gene transcription through epigenetic mechanisms (*15-17*). Succinate dehydrogenase (SDH)/complex II consists of four subunits (SDHA-D) that function in both the TCA cycle and the electron transportation chain (ETC). Its enzymatic activities that convert succinate to fumarate are coupled with reducing FAD to FADH2 and transferring an electron (complex II) into the ETC. Thus, SDH -dependent metabolic reaction represents a critical branch point in the TCA cycle. SDH is also a tumor-suppressor since inactivating SDH subunits leads to a spectrum of hereditary tumors, suggesting that inactivating this enzyme can confer survival and proliferation advantages to tumor cells (*18, 19*).

As activated T cells share metabolic characteristics with tumor cells (*1, 20*), we sought to investigate the role of SDH in T cells. Here, we reported that the TCA cycle enzyme SDH was indispensable for driving T cell proliferation by funneling carbon to support anabolic processes. In addition, the TCA cycle flux was constricted based on the availability of succinate that promotes the expression of pro-inflammatory genes through changing the T cell epigenome. Our findings implicated a role of the SDH/complex II in coupling the central carbon metabolism to epigenetic regulation to regulate T cell proliferation and inflammation coordinately.

Results

SDHB is required for T cell proliferation and survival

Loss-of-function mutations in SDH lead to a spectrum of hereditary tumors, suggesting that the resulting truncated TCA cycle can confer survival and proliferation advantages to tumor cells (*18*, *19*). Active T cells share metabolic characteristics with tumor cells and, therefore, may survive and proliferate in the absence of SDH activities (*21*). The critical functions of the TCA cycle include producing energy through coupling with the oxidative phosphorylation and generating biosynthetic precursors through cataplerosis (*11*). Accordingly, activated T cells could rapidly incorporate glucose- and glutamine-derived carbons into the TCA cycle metabolites and amino acids, indicating a robust TCA cycle coupled with anaplerosis and cataplerosis (**Fig. S1A-C**). SDH inhibitors with distinct modes of inhibition (*22*, *23*) significantly suppressed proliferation and decreased cell viabilities after T cells activation (**Fig. S2A-D**). To further illustrate the role of SDH in T cells, we generated a T cell-specific *SDHB* knockout mouse strain (*SDHB* cKO) by crossing the $SDHB^{fl}$ mouse strain with the CD4-Cre mouse strain. qPCR and immune blot (IB) analyses validated the deletion of SDHB (**Fig. 1A**), and SDH ablation resulted in a partially truncated TCA cycle, as evidenced by the accumulation of succinate and reduction of fumarate (**Fig. 1B**). While SDHB deletion did not result in any defects in T cell development in the thymus, it did reduce the percentage of T cells, particularly CD8 T cells, in the spleen and lymph node (**Fig. S3A**). In addition, the percentage of naturally occurring interferon-γ (IFN-γ) producing, interleukin-17 (IL-17) producing, and $Foxp3^+$ $CD4^+$ T cells were comparable in both wild-type (WT) and *SDHB* cKO mice (**Fig. S3B**). SDHB deletion in T cells significantly delayed cell cycle progression from G0/1 to S phase (**Fig.1C**), suppressed proliferation (**Fig.1D**), induced more cell death and reduced cell numbers (**Fig.1 E-F, S3C)**, which were associated with

moderately reduced cell surface activation markers (**Fig. S3D**), cell size (**Fig. S3E**), and protein content (**Fig. S3F**).

To assess the impact of ablating SDHB on $CD4^+$ T cells *in vivo*, we first employed a well-established competitive homeostatic proliferation assay to determine the ratio and carboxyfluorescein succinimidyl ester (CFSE) dilution pattern of purified WT*(Thy1.1$^+$)* or *SDHB cKO(Thy1.2$^+$)* $CD4^+$ T cells in a lymphopenic host (*Rag$^{-/-}$*). Both the ratio between wild type (WT*)* and *SDHB cKO* $CD4^+$ T cells and CFSE dilution patterns suggested that the loss of SDHB dampens T cell proliferation *in vivo* (**Fig.1G, S3G and S4A**). Next, we measured antigen-specific, TCR-dependent proliferation of WT or *SDHB* cKO $CD4^+$ T cells. We crossed *Thy1.1* and CD4-Cre, *SDHB^{fl}* mice with OT-II transgenic mice to generate WT(*Thy1.1$^+$*) and *SDHB cKO(Thy1.2$^+$)* donor OT-II strains in $CD45.2^+$ background. We then adoptively transferred CFSE labeled WT and *SDHB* cKO $CD4^+$ T cell into $CD45.1^+$ mice immunized with chicken ovalbumin ($OVA_{323-339}$). Consistent with the homeostatic proliferation results, *SDHB cKO* OT-II specific $CD4^+$ T cells displayed a significant proliferation defect in an antigen-specific manner after immunization (**Fig. 1H, S3H and S4B**). Experimental autoimmune encephalomyelitis (EAE), an inflammatory demyelinating disease model, is induced by active immunization with myelin-oligodendrocyte-glycoprotein (MOG) (**Fig.1I**). We used this well-characterized system to investigate the *in vivo* $CD4^+$ T cell response in *SDHB* cKO mice. In line with our homeostatic and antigen-specific proliferation results, the genetic deletion of SDHB in T cells protected the pathogenic progression of mice (**Fig.1I**) and dramatically reduced leukocyte infiltration (**Fig. 1J**), indicating that the dominant phenotype of SDH-deficient T cells in this model was the proliferation defect. Collectively, these findings suggested that ablating SDH/complex II activities significantly dampened T cell proliferation and *survival in vitro* and *in vivo*.

SDH inactivation decouples the TCA cycle from nucleoside biosynthesis

While an essential function of the TCA cycle is to sustain the oxidative carbon flux to meet energy consumption needs, the metabolic flux via the TCA cycle is also critical for carbon allocation, ensuring that biosynthetic precursors production is coupled with nutrient catabolism (*11-12*). Activated *SDHB* cKO T cells consistently displayed lower catabolic activities, such as glycolysis, pentose phosphate pathway (PPP), glutamine oxidation, but not fatty acid oxidation (FAO) as compared with WT active T cells (**Fig. 2A-D**). Since glutamine is a major carbon source for replenishing the TCA cycle intermediate metabolite α-ketoglutarate (α-kg) in T cells after activation (*24*), we supplied $^{13}C_5$-glutamine as a metabolic tracer in T cell culture media and followed ^{13}C incorporation into downstream metabolites in T cells after activation. The $^{13}C_4$ isotopologue of succinate was accumulated, but the corresponding $^{13}C_4$ or $^{3}C_3$ isotopologues of downstream metabolites including fumarate, malate, aspartate, and pyrimidine nucleotides were significantly reduced in activated *SDHB* cKO T cells as compared with activated WT T cells (**Fig. 2E**). SDHB deficiency reduced the level of intracellular aspartate (**Fig. 2E**), which is produced from the TCA cycle metabolite (oxaloacetate) and consequently utilized for nucleotide and DNA/RNA biosynthesis (*11-12*). Notably, the incorporation of carbon from ^{14}C-glutamine into RNA and DNA was significantly suppressed in activated *SDHB* cKO T cells as compared with activated WT T cells (**Fig. 2F**). Metabolite profiling also revealed a global decrease of intracellular pyrimidine nucleotides, purine nucleotides, and their precursors in activated *SDHB* cKO T cells (**Fig. 2G**). Finally, the overall DNA/RNA content was lower in *SDHB* cKO T cells than WT T cells after activation (**Fig. 2H**). Collectively, our metabolic experiments have shown that the carbon flux from glutamine to the TCA cycle intermediate metabolites, nucleotides and

DNA/RNA biosynthesis was dampened in the absence of SDH/complex II activity.

Nucleosides supplementation partially compensates for the loss of de novo biosynthesis of nucleotides in *SDHB* cKO T cells

We then sought to determine the importance of SDH in directing TCA cycle carbon flow to nucleotide biosynthesis for supporting T cell proliferation. Since cells could directly utilize nucleosides through salvage pathway, we reasoned that providing nucleosides could bypass the block in de novo synthesis and consequently overcome some of the T cell defects caused by SDHB deficiency. Indeed, supplementation with a mixture of nucleosides (adenosine, uridine, guanosine, thymidine, cytidine, inosine) partially restored the viability and proliferation of *SDHB* cKO T cells after activation (**Fig. 3A-D**), which was accompanied by partial restoration of DNA/RNA content (**Fig. 3E**) and promoted cell cycle progression from G0/1 to S phase (**Fig. 3F**). Nucleosides supplement did not affect WT cells growth and proliferation (**Fig. 3A-D**). In addition, adding inosine together with pyrimidines (thymidine, cytidine, and uridine) maximized the rescue effect (**Fig. 3G-J**), demonstrating the importance of SDH in supporting both purine and pyrimidine biosynthesis.

Nucleotide pool imbalance can cause DNA damage and, consequently, induce apoptosis (*25*). In support of this concept, SDHB deletion led to high levels of DNA damage marker (phosphor-histone H2AX), and nucleosides supplementation reversed this effect (**Fig. S5A-B**). Accordingly, the pan-caspase inhibitor (QVD) enhanced the cell viability but not the proliferation of *SDHB* cKO T cells (**Fig. S5C-E**). The combination of nucleosides supplementation and QVD further enhanced the viability but not the proliferation of *SDHB* cKO T cells (**Fig. S5C-E).** A defective SDH/complex II can increase ROS production (*26*). However, we only observed a moderate

induction of mitochondrial ROS in *SDHB* cKO T cells (**Fig. S5F**). ROS scavengers failed to rescue cell viability and proliferation defects in *SDHB* cKO T cells (**Fig. S5G-I**).

To ensure no phenotypic discrepancies between genetic modulation of different subunits of SDH in T cells, we generated a T cell-specific SDHD knockout strain (*SDHD* cKO) by crossing CD4-Cre mice with previously reported *SDHD*^{fl} mice (*27*). Similar to the effect of SDHB deletion in T cells, SDHD deletion reduced the percentage of T cells in the spleen and lymph node without causing defects in T cell development in the thymus (**Fig. S6A-B**). SDHD deletion significantly suppressed proliferation and caused more death after T cells activation, which could be partially reversed by nucleosides supplementation (**Fig. S6C-F**). Next, we examined the effect of SDH deficiency on T cell survival and proliferation under polarization conditions. Both SDHB and SDHD deficiency resulted in cell survival and proliferation defects in T helper 1 (T_H1) (**Fig. S7 A-B**) and T helper 17 (T_H17) (**Fig. S7 C-D**) polarization conditions. Together, our data suggested that a crucial role of the TCA cycle in supporting T cell proliferation was to allocate carbon for nucleotides biosynthesis (**Fig. S7E**).

SDH inactivation results in a pro-inflammatory gene signature in T cells after activation

To gain more mechanistic insights into the effects of SDHB deletion on T cells, we performed RNA-seq in activated WT and *SDHB* cKO T cells, which revealed an enriched pro-inflammatory gene signature in *SDHB* cKO T cells after activation (**Fig. 4A-C**). Active *SDHB* cKO T cells, but not naïve, expressed higher levels of four representative pro-inflammatory genes, including *Il17a*, *Il17f, Ifng*, and *Il22,* than WT T cells, indicating that TCR activation is required to achieve an enriched pro-inflammatory gene signature in *SDHB* cKO T cells (**Fig. 4D**). Consistent with gene expression data, the culture media collected from *SDHB* cKO T cells contained

significantly higher levels of pro-inflammatory cytokines than the culture media collected from WT T cells (**Fig. S8A**). Nucleosides supplementation, which could partially rescue cell proliferation and survival (**Fig. 3 A-D**), failed to reduce the pro-inflammatory cytokine expression in *SDHB* cKO T cells (**Fig. 4E**). Also, the culture media collected from *SDHB* cKO T cells could not increase pro-inflammatory gene expression in WT T cells (**Fig. 4F**). Thus, a cell-intrinsic mechanism that is unrelated to changes in proliferation and survival or secretory molecules was responsible for the pro-inflammatory gene signature in *SDHB* cKO T cells after activation.

The increasing intracellular succinate/α-KG ratio promotes the expression of pro-inflammatory genes in *SDHB* cKO T cells after activation

SDHB deficiency reciprocally increased the level of succinate while reducing α-KG in T cells after activation (**Fig. S8B**). Such an increased succinate/α-KG ratio suppressed the enzymatic activities of the dioxygenase family, impacting the hypoxia signaling response and DNA/histone methylation pattern (**Fig. 5A**), both of which may lead to a pro-inflammatory response (*28-30*). Correspondingly, cell-permeable succinate (*22*) increased succinate/α-KG ratio (**Fig. S8C**) and partially mimicked the effect of SDHB-deficiency on upregulating pro-inflammatory genes in WT T cells after activation (**Fig. 5B**). Conversely, cell-permeable α-KG (dimethyl- α-KG) decreased the succinate/α-KG ratio (**Fig. S8C**) and reduced the level of pro-inflammatory genes in *SDHB* cKO T cells after activation (**Fig. 5C**). Similarly, a glutamate dehydrogenase inhibitor (R162), which could reduce glutamine-derived anaplerotic flux to attenuate succinate buildup, decreased the expression of pro-inflammatory genes in *SDHB* cKO T cells after activation (**Fig. 5D**). Finally, SDHD deficiency phenocopied SDHB deficiency in inducing pro-

inflammatory gene expression, which was reversed by cell-permeable α-KG (**Fig. S8D**). Next, accessed the effects of changing the succinate/α-KG ratio on $CD4^+$ T cell differentiation. The succinate/α-KG ratio in proinflammatory T cell lineages (T_H1 and T_H17) was higher than either uncommitted lineage (T_H0) or anti-inflammatory lineage (iT_{reg}) (**Fig. S8E**), indicating that increasing the succinate/α-KG ratio might promote T_H1 and T_H17 differentiation. Indeed, cell-permeable succinate enhanced pro-inflammatory T_H1 and T_H17 cell differentiation, which could be reversed by cell-permeable α-KG (**Fig. 5E-F**). Similarly, cell-permeable 2-hydroxyglutarate (L-octyl-L2HG) that increased intracellular 2-HG levels to antagonize α-KG dependent dioxygenases (*31*) enhanced T_H1 and T_H17 differentiation. Cell-permeable α-KG could partially reverse the effect of 2-HG on T cell differentiation (**Fig. S9A-B**). *SDHB* cKO T cells failed to proliferate and could not generate IFN-γ^+ $CD4^+$ T cells under T_H1 polarization conditions or IL-17^+ $CD4^+$ T cells under T_H17 polarization conditions (**Fig. S9C**). These results are in line with previous observations that cell proliferation is required to achieve optimized T cell polarization (*32*). Genomic deletion and RNA depletion of SDHB require a specific time after Cre activation. Also, the protein half-life of SDHB is around 10 hrs (*33*). We envisioned that a tamoxifen-inducible Cre recombinase (CreERT2) model might allow us to bypass the effect of SDHB deficiency on T cell activation and proliferation if Cre functions during activation. Compared with WT cells, acute deletion of SDHB largely bypassed its requirement for driving cell proliferation but enhanced T_H1 and T_H17 differentiation (**Fig. S9D-E**). Cell-permeable α-KG eliminated the effects of acutely deleting SDHB on T cell differentiation (**Fig. S9D-E**). Using CreERT2 model, we have differentiated the role of SDH in regulating T cell activation and proliferation from its role in driving T cell differentiation. Together, our results suggested that increasing the succinate/α-KG ratio promoted pro-inflammatory gene expression and enhanced

T_H1 and T_H17 differentiation *in vitro*.

HIF1-α is dispensable for enhanced pro-inflammatory gene signature in *SDHB* cKO T cells

An increased succinate/α-KG ratio suppressed enzymatic activities of the α-KG -dependent dioxygenases, which include prolyl hydroxylases, Ten-eleven translocation (TET) enzymes, and lysine demethylases, and may consequently impact inflammation via HIF-1a and/or epigenetic mechanism (**Fig. 5A**) (*34*, *35*). HIF1-α plays a role in enhancing inflammation in T cells and other immune cells (*36*-*38*). To determine if HIF1-α is responsible for upregulating pro-inflammatory genes, we generated a T cell-specific *SDHB* and *HIF1-α* double knockout (dKO) strain by crossing the *HIF1-α*^{fl} with CD4-Cre, *SDHB*^{fl} strain. *HIF1-α/SDHB* dKO T cells displayed comparable phenotypes in T cell development, cell survival and proliferation compared with *SDHB* cKO T cells after activation (**Fig. S10A-F**). Pro-inflammatory gene expression was not reduced in *HIF1-α/SDHB* dKO T cells compared to *SDHB* cKO T cells after activation (**Fig. S10G**). Conversely, cell-permeable succinate could enhance T_H1 and T_H17 cell differentiation in a HIF1-α independent manner (**Fig. S11A-B**). Collectively, our results suggested that HIF1-α did not mediate pro-inflammatory phenotypes in *SDHB* cKO T cells after activation.

SDHB deficiency promotes a pro-inflammatory gene signature through regulating chromatin accessibility and pro-inflammatory transcription factors

Next, we measured succinate, α-KG, DNA, and histone methylation levels in WT and *SDHB* cKO naïve T cells. Compared with the WT T cells, the *SDHB* cKO naïve T cells contained a higher level of succinate but not α-KG than WT T cells (**Fig. S12A**). In contrast to control T

cells, the *SDHB and SDHD* cKO T cells or T cells treated with cell-permeable succinate displayed higher levels of 5-methylcytosine (5-mC) and histone methylations in several key lysine residues that are often associated with transcriptional activities (*39*, *40*) (**Fig. S12 B-F**). We reasoned that the DNA and histone methylations might work in concert to reprogram an epigenetic state via modulating chromatin accessibility, consequently leading to induction of inflammatory genes in activated T cells with succinate accumulation. To test this hypothesis, we examined the genome-wide transcriptomes and chromatin-accessibility by performing RNAseq and Assay for Transposase Accessible Chromatin with high-throughput sequencing (ATAC-seq) in parallel in activated $CD4^+$ WT and *SDHB* cKO T cells. Indeed, ATAC-seq revealed distinctive patterns of DNA accessibility that were associated with genomic loci of genes involved in T cell activation and inflammation in activated WT and *SDHB* cKO $CD4^+$ T cells (**Fig. 6A-B**). After integrating the RNA-seq and ATAC-seq data, we found that the induction of pro-inflammatory genes and transcription factors known to regulate T cell differentiation and inflammation were concordant with the increase in chromatin accessibility of these genes in the activated *SDHB* cKO $CD4^+$ T cells (**Fig. 6C**). PR domain zinc finger protein 1 (*Prdm1*) was among these genes with increased transcript and DNA accessibility. *Prdm1* encodes B-lymphocyte-induced maturation protein (Blimp-1), a transcription factor known which is co-localized with STAT-3, p300, RORγt on the Il23r, Il17f, and Csf2 cytokine loci to regulate T cell differentiation and inflammation (*41*, *42*). Analysis of transcriptional factor binding motifs in the differential accessibility regions revealed that *Prdm1* was one of the top transcription factors that may gain increased chromatin accessibility at the regulatory elements of the T cell activation and inflammation genes in the activated *SDHB* cKO $CD4^+$ T cells (**Fig. 6D**). In addition, ATAC-seq analysis of T cells of WT and *SDHB* cKO under naïve conditions also showed a significant motif

enrichment of *Prdm1* in the differential accessibility regions, portending the increased transcription of its target gene upon stimulation (**Fig. S12G-H**). We, therefore, hypothesized that transcription factors, such as *Prdm1* that showed concordant increases in both their expression level and DNA accessibility, may play a key role in driving inflammation in *SDHB* cKO $CD4^+$ T cells. Among a panel of transcription factors that displayed enhanced DNA accessibility in either activated or naïve *SDHB* cKO $CD4^+$ T cells (**Fig. 6D and S12G)**, *Prdm1*'s expression was enhanced by cell-permeable succinate and SDHB deletion (**Fig. 6E-G)**. Moreover, cell-permeable α-KG reduced the expression of *Prdm1* in *SDHB* cKO $CD4^+$ T cells (**Fig. 6E-F**).

Next, we employed a CRISPR-Cas9 approach to testing if *Prdm1* was required for regulating the expression of inflammatory genes and T cell differentiation in the context of SDHB deletion and succinate accumulation. Indeed, the deletion of *Prdm1* reduced the level of pro-inflammatory genes *Il17a*, *Il17f, Ifng,* but not *Il22* in *SDHB* cKO T cells (**Fig. 7A-B)**. Moreover, deletion of *Prdm1* eliminated the effect of cell-permeable succinate on promoting T_H1 and T_H17 differentiation (**Fig. 7C-D**). Collectively, these results suggested that TCA cycle metabolites (succinate/α-KG) regulated T cell inflammation through a coordinated epigenetic and transcriptional control of inflammatory genes.

Changing the succinate/α-KG ratio regulates *Prdm1*/Blimp-1 expression and T cell differentiation through an epigenetic mechanism

Next, we assessed the effect of modulating the succinate/α-KG ratio on *Prdm1*/Blimp-1 expression and T cell differentiation. Cell-permeable α-KG moderately reduced *Prdm1*/Blimp-1 expression under T_H1 and T_H17 polarization conditions (**Fig. S13A-B**). Similarly, treating T cells with a competitive inhibitor of SDH (NV161) (*22, 43*) in a dose without significantly

compromising cell proliferation (**Fig. S13C**) enhanced T_H1 and T_H17 differentiation and *Prdm1*/Blimp-1 expression (**Fig. S13D-G**). In line with the effect of acutely deleting SDHB on T cell differentiation (**Fig. S9D-E**), acutely deleting SDHB increased *Prdm1*/Blimp-1 expression under T_H1 and T_H17 polarization conditions, which could be reversed by cell-permeable α-KG (**Fig. S13H-I**). We reasoned that H3K4me3 might play a role in regulating *Prdm1*. Indeed, chromatin immunoprecipitation (ChIP)-qPCR revealed that the H3K4me3 signal was higher in *SDHB* cKO than WT $CD4^+$ T cells (**Fig. S14A**). The state of H3K4me3 is determined by the lysine-specific demethylase 5 (KDM5) family and the histone methyltransferase, mixed-lineage leukemia 1 (MLL1) (*44*, *45*). Inhibiting KDM5 by C70 (*46*) increased the level of H3K4me3, accompanied by increased expression of *Prdm1* in WT $CD4^+$ T cells following activation (**Fig. S14 B-D**). Conversely, inhibiting MLL1 by MM102 (*47*) reduced the level of H3K4me3 and the expression of *Prdm1* in *SDHB* cKO $CD4^+$ T cells (**Fig. S14B and S14E-F**). Moreover, inhibiting KDM5 by C70 increased the level of H3K4me3 under T_H1 and T_H17 polarization conditions, accompanied by enhanced differentiation (**Fig. S14G-J**). Conversely, inhibiting MLL1 by MM102 reversed the effects of acutely deleting SDHB on H3K4me3 during T_H1 and T_H17 differentiation (**Fig. S15A-H**). Together, these results indicated that changing the succinate/α-KG ratio might regulate *Prdm1* expression and T cell differentiation through modulating the level of H3K4me3.

Discussion

We revealed a critical role of SDH/complex II in allocating carbon resources for anabolic processes and epigenetic regulation in T cell proliferation and inflammation. Rapidly evolving pathogens impose selective pressures on host immune cells' metabolic fitness and metabolic plasticity, allowing immune cells to maintain homeostasis while remaining ready to mount rapid responses under diverse metabolic and immune conditions (*48-51*). Beyond this, the availability of specific metabolites and the pathways that process them interconnect with signaling events and epigenetic regulators in the cell, orchestrating metabolic checkpoints that influence T cell activation, differentiation, and immune function (*1-3, 52-57*). While the essential function of the TCA cycle is to sustain the oxidative carbon flux to meet energy consumption needs, the metabolic flux via the TCA cycle is also critical for carbon anabolism, ensuring that production of biosynthetic precursors of protein, lipids, and DNA/RNA is coupled with energy production from nutrients to sustain cell growth. Accordingly, the major role of the ETC in supporting cell proliferation is to regenerate nicotinamide adenine dinucleotide (NAD)+ and to permit aspartate synthesis in cancer cells (*55, 58-60*). Similarly, we found that carbon input (mainly through glutamine) to replenish TCA cycle intermediates (anaplerosis) was balanced with an output of 4-carbon intermediates from the TCA cycle to aspartate and nucleosides and nucleotides (cataplerosis) in T cells. These results suggest that active T cells share metabolic characteristics with tumor cells (*1, 20*).

Unlike hyper-proliferative tumor cells, where inactivating the TCA cycle enzymes SDH can confer survival and proliferation advantages to tumor cells (*18, 19*), we found that SDH-dependent steps were vital for carbon allocation via the TCA cycle in supporting anabolic

processes to drive T cell proliferation. The additional genetic alterations may confer a high degree of metabolic adaptation to SDH/complex II deficient cancer cells (*61, 62*). Inhibiting SDH suppresses T-cell inflammation and macrophages(*21, 63, 64*). In contrast, we found that increasing the succinate/α-KG ratio by inhibiting SDH or providing cell-permeable metabolites promoted T cell inflammation and differentiation. Since different approaches, materials, and cell types were used and studied across our studies and previous studies, we reasoned that the combination of multiple factors, including differences in pharmacological reagents, genetic approaches, cellular and biological contexts, caused the discrepancies between our findings and previous findings.

Succinate is necessary to promote inflammation during macrophage activation (*65, 66*). Endogenous metabolite itaconate regulates inflammatory cytokine production during macrophage activation by targeting SDH/complex II, implicating metabolites as key regulation signals (*63, 67, 68*). In macrophages, succinate exerts its pro-inflammatory actions through a plethora of mechanisms, including stabilizing HIF-1α, affecting mitochondrial ROS (mtROS) production, and activating cell surface receptor, the G-protein coupled receptor succinate receptor 1 (SUCNR1) (*36, 63, 69, 70*). In T cells, the TCA cycle allocates carbon inputs to modulate substrates, antagonists, and cofactors of epigenetic-modifying enzymes, thereby enacting epigenetic changes during T cell activation (*15-17*). Particularly, succinate is a critical metabolite regulator of histone and DNA demethylases (*12, 15-17*). We found that the succinate/α-KG ratio in proinflammatory T cell lineages (T_H1 and T_H17) was higher than either uncommitted lineage (T_H0) or anti-inflammatory lineage (iT_{reg}), indicating that a higher succinate/α-KG ratio might be required for the differentiation of proinflammatory T cell

lineages.

T cell activation is accompanied by a dynamic remodeling of chromatin, accessibility, and histone modifications, which determine the transcriptional signatures of lineage-specifying genes via cell type-specific gene regulatory elements. The epigenetic landscape promotes the faithful execution of lineage-restricting transcription programs while maintaining a degree of plasticity in response to intracellular and environmental cues (*9, 10*). Mitochondrial complex III regulates T cell activation and regulatory T cell functions through controlling mitochondria ROS and DNA methylation, respectively (*1, 71*). We uncovered distinctive patterns of DNA accessibility that were associated with genomic loci of inflammatory genes and transcription factors that regulate inflammatory genes in WT and *SDHB* cKO $CD4^+$ T cells.

We observed a concordant increase in the expression and the motif accessibility of transcription factor *Prdm1*, a known regulator of T cell differentiation and inflammation, in *SDHB* cKO $CD4^+$ T cells compared to WT $CD4^+$ T cell (*41*). Succinate accumulation may have induced *Prdm1* expression via an H3K4me3-dependent mechanism. Moreover, deletion of *Prdm1* eliminated the effect of succinate on promoting the expression of the inflammatory genes and effector T cell differentiation. However, epigenetic regulation of multiple other genes was also involved in mediating the effect of succinate in promoting T cell inflammation. In addition to *prdm1*, several other transcription factors known to regulate T cell differentiation and inflammation also displayed enhanced DNA accessibility and expression in the activated *SDHB* cKO CD4 T cells. These results supported the idea that SDH/complex II was necessary for promoting T cell inflammation through a coordinated epigenetic and transcriptional control of inflammatory

genes.

Collectively, TCA cycle flux and the ETC may act concertedly to ensure coordinated carbon assimilation, energy production, and epigenetic regulation. The participation of the master transcription factor such as *Prdm1* in such combinational contort adds one layer of regulatory flexibility on cells, permitting contextual gene expression patterns. This mechanism in T cells may provide some insights to explain how metabolic constraints impose on the epigenetic and transcriptional regulation of a broad range of cell-fate transitions.

Materials and Methods.

Study design

This study investigates the function of Complex II/SDH in T cells. We assessed the T cell survival, activation, proliferation, differentiation, and inflammation in the context of inhibiting or enhancing SDH activities through a combination of genetic, pharmacological, and metabolic approaches. For each experiment, n values and the number of experimental replicates are specified in corresponding figure captions. In murine experiments, males and females were used in equal proportions.

Mice

Mice with one targeted allele of *SDHB* on the C57BL/6 background (*SDHB*$^{tm1a(EUCOMM)Hmgu}$) were generated by The European Conditional Mouse Mutagenesis Program (EUCOMM) (*72*). The mice were first crossed with a transgenic Flippase strain (B6.129S4*Gt(ROSA)26Sor*$^{tm1(FLP1)Dym}$/RainJ) to remove the LacZ-reporter allele and then crossed with the CD4-Cre strain to generate T cell-specific *SDHB* knockout strain (*SDHB* cKO). *SDHB*^{fl} were crossed with ROSA26CreERT2 to generate the acute deletion model. Mice with one targeted allele of *SDHD* on the C57BL/6 background were crossed with the CD4-Cre strain to generate the CD4Cre *SDHD* cKO mice (*SDHD* cKO) (*27*). *SDHB*^{fl} were crossed with CD4Cre *HIF1-α* KO mice (*73*) to generate T cell-specific *SDHB* and *HIF1-α* double knockout (dKO) strain. OT-II mice (B6.Cg-Tg(TcraTcrb)425Cbn/J) were crossed with CD4Cre *SDHB* cKO mice to generate the OT- II CD4Cre *SDHB* cKO mice. OT-II mice (B6.Cg-Tg(TcraTcrb)425Cbn/J) were crossed with *Thy1.1*$^{+}$ mice (B6.PL-*Thy1*a/CyJ) to generate OT-II *Thy1.1* mice. C57BL/6 (WT) mice, CD45.1^{+} mice (B6.SJL-Ptprca Pepcb/BoyJ), and Rag1-/- mice (B6.129S7-

Rag1tm1Mom/J) were obtained from the Jackson Laboratory (JAX, Bar Harbor, ME). Mice with gender and age-matched (7-12 weeks old) were used in the experiments. All mice were bred and kept in specific pathogen-free conditions at the Animal Center of Abigail Wexner Research Institute at Nationwide Children's Hospital. Animal protocols were approved by the Institutional Animal Care and Use Committee of the Abigail Wexner Research Institute at Nationwide Children's Hospital (IACUC; protocol number AR13-00055).

Mouse T cell isolation and culture

Total $CD3^+$ T cells or naïve $CD4^+$ T cells were enriched from mouse spleen and lymph nodes by negative selection using MojoSort Mouse CD3 T Cell Isolation Kit or MojoSort Mouse CD4 Naive T Cell Isolation Kit (MojoSort, Biolegend). Isolated T cells (1×10^6 cells/mL) were maintained in culture media containing mouse IL-7 (5 ng/mL) for naïve condition or stimulated with mouse IL-2 (100 U/mL) as well as plate-bound anti-mCD3 and anti-mCD28 antibodies for activation condition. Culture plates were pre-coated with 2 μg/mL anti-mCD3 (clone 145-2C11, Bio X Cell) and 2 μg/mL anti-mCD28 (clone 37.51, Bio X Cell) antibodies overnight at 4°C.
For T cell's CFSE dilution analysis, $1\text{-}2 \times 10^7$ cells were incubated in 4 μM PBS-diluted CFSE (Invitrogen) for 10 min; cells were then washed three times with RPMI-1640 medium containing 10% FBS for culture.
For $CD4^+$ T cell differentiation, freshly isolated naïve $CD4^+$ T cells (0.6×10^6/mL) were stimulated with plate-bound antibodies and with mIL-2 (200 U/mL), mIL-12 (5 ng/mL, PeproTech) for T_H1 differentiation, with mIL-6 (50 ng/mL, PeproTech), hTGF-β1 (2 ng/mL), anti–mIL-2 (8 μg/mL, Bio X Cell), anti–mIL-4 (8 μg/mL, Bio X Cell), and anti–mIFN-γ (8 μg/mL, Bio X Cell) for T_H17 differentiation, or with mIL-2 (200 U/mL) and hTGF-β1 (5 ng/mL,

PeproTech) for iTreg differentiation. Of note, 48 wells culture plates were pre-coated with 5 μg/mL anti-mCD3 (clone 145-2C11, Bio X Cell) and 5 μg/mL anti-mCD28 (clone 37.51, Bio X Cell) antibodies over night at 4°C for T_H1 and iTreg polarization or were pre-coated with 10 μg/mL anti-mCD3 (clone 145-2C11, Bio X Cell) and 10 μg/mL anti-mCD28 (clone 37.51, Bio X Cell) antibodies over night at 4°C for T_H17 polarization. At day 3, eBioscience™ Cell Stimulation Cocktail of phorbol 12-myristate 13-acetate (PMA), ionomycin, brefieldin A and monensin (eBioscience) were added into T_H1 or T_H17 cells for 4 h followed by intracellular detection of cytokines.

All cells were cultured in RPMI 1640 media supplemented with 10% (v/v) heat-inactivated dialyzed fetal bovine serum (DFBS), 2 mM L-glutamine, 0.05 mM 2-mercaptoethanol, 100 units/mL penicillin and 100 μg/mL streptomycin at 37˚C in 5% CO2. Single nucleosides (NS) including Adenosine (A), Uridine (U), Inosine (I), Cytidine (C), Guanosine (G), Thymidine (T) were diluted in water and mixed to reach a final concentration of 300μM NS mixture, 200μM TCUI combination or 150 μM TCU combination (50μM for each), Atpenin A5 (A5, 100nM), diacetoxymethyl malonate (NV161, 50-100μM), dimethyl-itaconate (DI, 0.5mM), or 4-octyl-itaconate (4OI, 500μM), 20uM QVD-OPh, 1mM NAC, 1mM GSH EE, 100μM or 25 μM NV118, 10mM or 2mM dimethyl α-ketoglutarate (α-KG), 1μM L(S)-2HG, 50μM R162, 600nM 4OHT, 10-25μM MM102, or 5-10μM KDM5-C70 were used in the indicated experiments. All reagents, including cytokines, antibodies, inhibitors, and chemicals, are listed in supplemental table 1.

Flow Cytometry

For analysis of surface markers, cells were suspended in phosphate-buffered saline (PBS) containing 2% (w/v) bovine serum albumin (BSA) and incubated with antibodies (supplemental

Table 2) for 30 min at 4°C. Cells were washed and stained with 7AAD (Biolegend) for cell viability analysis for 5 min before running on a flow cytometer. For intracellular staining, cells were collected and stained with surface markers first. Then cells were stimulated with (for cytokines staining) or without (for non-cytokine proteins staining) stimulation cocktails followed by fixation and permeabilization using FoxP3 Fixation/Permeabilization Kit (eBioscience) and staining of intracellular proteins. For DNA methylation assay, cells were harvested, washed with PBS, and fixed with 4% paraformaldehyde for 15 min at room temperature. After washing with PBS, cells were permeabilized by 0.5% Triton X-100 in PBS for 15 min at room temperature, then incubated in 2 N HCl for 30 min at 37°C. Then, cells were neutralized with 100 mM Tris HCl pH 8.8 for 10 min followed by extensive washes with 0.05% Tween 20 in PBS and blocking in 1% BSA and 0.05% Tween 20 in PBS for 2 h. Cells were incubated with the anti-5-methylcytosine (5-mC) antibody for 1 h, followed by 7AAD staining for 5 min for DNA content analysis (*74*). For histone methylations assay, cells were collected and stained with surface markers, then were fixed and permeabilized using the FoxP3 Fixation/Permeabilization Kit (eBioscience). Cells were incubated with a primary monoclonal antibody for 1 h at room temperature, washed with staining buffer, and incubated with a secondary antibody (Alexa-Fluor 647- or Alexa-Fluor 405-conjugated goat anti-mouse Ig antibodies; Invitrogen, France) for 45 min at room temperature. Histone methylation levels were normalized to the level of total H3. Flow cytometry antibodies are listed in supplemental Table 2. For DNA/RNA content assay, cells were collected and stained with surface markers, then were fixed with 4% paraformaldehyde for 30 min at 4°C and permeabilized with FoxP3 permeabilization solution (eBioscience). Cells were stained with 7AAD for 5 minutes and then stained with pyronin-Y (4ug/ml, PE) for 30 minutes. Cells were washed and then analyzed by flow cytometer using PE channel for pyronin-

Y and PerCP channel for 7AAD. Protein synthesis assay kit (Item No.601100, Cayman) was used for protein content assay. Cells were incubated in O-propargyl-puromycin (OPP) for 1 h, then were fixed and stained with 5 FAM-Azide. Cells were then washed and analyzed by flow cytometer using FITC channel. For Cell cycle analysis, cells were incubated with 10 μ g/mL BrdU for 1 hr, followed by surface staining, fixation, and permeabilization according to the manufacturer's (Phase-Flow Alexa Fluro 647 BrdU Kit, Biolegend). Cells were then stained with antibodies against BrdU and 7AAD. Flow cytometry data were acquired on Novocyte (ACEA Biosciences) and were analyzed with FlowJo software (BD Biosciences).

Western blot analysis

For protein extraction, cells were harvested, lysed, and sonicated at 4℃ in a lysis buffer (50 mM Tris-HCl, pH 7.4, 150 mM NaCl, 0.5% SDS, 5 mM sodium pyrophosphate, protease, and phosphatase inhibitor tablet). Cell lysates were centrifuged at 13,000 × g for 15 min, and the supernatant was recovered. The protein concentrations were determined using the Pierce™ BCA Protein Assay kit (Thermo Fisher Scientific). The samples were boiled in NuPAGE® LDS Sample Buffer and Reducing solution (Thermo Fisher Scientific) for 5 min. The proteins were separated by NuPAGE 4-12% Protein Gels (Thermo Fisher Scientific), transferred to PVDF membranes by the iBlot Gel Transfer Device (Thermo Fisher Scientific), then incubated with primary antibodies (listed in supplemental Table 3), followed by incubating with the secondary antibodies conjugated with horseradish peroxidase. Immunoblots were developed on films using the enhanced chemiluminescence technique.

RNA extraction and RT-qPCR

RNeasy Mini Kit (Qiagen) was used for RNA isolation. Random hexamers and M-MLV Reverse Transcriptase (Invitrogen) was used for cDNA synthesis. BIO-RAD CFX96™ (or CFX384™) Real-Time PCR Detection System was used for SYBR green-based quantitative PCR. The relative gene expression was determined by the comparative *CT* method, also referred to as the $2^{-\Delta\Delta CT}$ method. The data were presented as the fold change in gene expression normalized to an internal reference gene (beta2-microglobulin) and relative to the control (the first sample in the group). Fold change = $2^{-\Delta\Delta C}{}_{T} = [(CT_{\text{gene of interest}} - CT_{\text{internal reference}})]$ sample A - $[(CT_{\text{gene of interest}} - CT_{\text{internal reference}})]$ sample B. Samples for each experimental condition were run in triplicated PCR reactions. Primers are listed in supplemental Table 4.

Radioactive tracer-based metabolic activity analysis.

The radioactive tracer-based metabolic assay was performed as described previously (*75*). Glycolysis was measured by the generation of $^{3}H_2O$ from [5-^{3}H(N)] D-glucose, fatty acid oxidation was measured by the generation of $^{3}H_2O$ from [9,10-^{3}H] palmitic acid, pentose phosphate pathway was measured by the generation of $^{14}CO_2$ from [1-^{14}C] D-glucose, glutamine oxidation activity was measured by the generation of $^{14}CO_2$ from [U-^{14}C]-glutamine. For catabolic activities generation of $^{14}CO_2$, five million T cells in 0.5 mL fresh media were dispensed into 7mL glass vials (TS-13028, Thermo) with a PCR tube containing 50µL 0.2N NaOH glued on the sidewall. After adding 0.5 µCi radioactive tracer, the vials were capped using a screw cap with a rubber septum (TS-12713, Thermo) and incubated at 37 ℃ for 2 hrs. The assay was then stopped by injection of 100µL 5N HCL into the vial. Vials were kept at room temperate overnight to trap the $^{14}CO_2$. The NaOH solution in the PCR tube was then transferred to scintillation vials containing 10mL scintillation solution for counting. A cell-free sample

containing the same amount of tracer was included as a background control. For catabolic activities generating $^{3}H_2O$, 1μCi radioactive tracer was added to the suspension of one million cells in 0.5mL fresh media in 48 wells, then incubated at 37 ℃ for 2 hrs. The assay was stopped by transferring samples to a 1.5 mL microcentrifuge tube containing 50μL 5N HCL, which was placed in a 20 mL scintillation vial containing 0.5 mL water. Then the vial was capped and sealed. $^{3}H_2O$ was separated from other radio-labeled metabolites by evaporation diffusion overnight at room temperature. The 1.5 mL microcentrifuge tube was removed, and 10mL scintillation solution was added to the vial before counting A cell-free sample containing 1μCi radioactive tracer was included as a background control. To examine the incorporation of glutamine-derived carbon into the DNA/RNA, 0.5mM glutamine and 2μCi [U-14C]-glutamine was added to 1.5 $X10^7$ cells suspended with a glutamine-free medium and cultured for 6 hrs with IL2. RNA and DNA were isolated with Quick-DNA/RNA™ Miniprep Kit (Cat#: D7005). Radioactivity was measured by liquid scintillation counting and normalized to total DNA or RNA concentration.

Adoptive cell transfer and *in vivo* proliferation

For homeostatic proliferation in lymphopenic *Rag*$^{-/-}$ mice, naïve $CD4^+$ T cells isolated from donor mice were mixed with WT and KO cells at a 1:1 ratio and labeled with CFSE. Approximately 1×10^7 cells in 150 μL PBS were transferred via retro-orbital venous injection into 6–8-week-old gender-matched host mice. Mice were sacrificed after 5 days, and lymph nodes were extracted from host mice, then processed for surface staining and flow analysis.

For antigen-driven proliferation using OTII mice, naïve $CD4^+$ T cells isolated from OTII/CD45.2 TCR transgenic donor mice were mixed with WT and KO cells at a 1:1 ratio and labeled with

CFSE. Approximately 1×10^7 cells in 150 μL PBS were transferred via retro-orbital venous injection into 6–8-week-old gender-matched CD45.1 host mice. Host mice were immunized subcutaneously in the hock area (50 μL each site) in both legs with 1 mg/mL $OVA^{323-339}$ peptide (InvivoGen) emulsified with CFA (InvivoGen). Mice were sacrificed after 7 days, and lymph organs were extracted from host mice then processed for surface staining, intracellular staining, and flow analysis.

Experimental Autoimmune Encephalomyelitis (EAE) Induction and Assessment

For induced EAE, mice were immunized subcutaneously with 100 μg of myelin oligodendrocyte glycoprotein $(MOG)_{35–55}$ peptide emulsified in complete Freund adjuvant (CFA), which was made from IFA(Difco) plus mycobacterium tuberculosis (Difco). Mice were i.p. injected with 200 ng of pertussis toxin (List Biological) on the day of immunization and 2 days later. The mice were observed daily for clinical signs and scored as described previously (*76*).

Histopathology

Mice were euthanized and perfused with 25 mL PBS with 2mM EDTA by heart puncture to remove blood from internal organs. Cervical spinal cords were collected, fixed by 10% neutral buffered formalin solution, and decalcified. Tissues were then embedded in paraffin, sectioned, and stained with standard histological methods for Haemotoxylin and Eosin (H&E) staining. Microscopy images were taken using Zeiss Axio Scope A1.

Metabolite quantification and stable isotope labeling

Gas Chromatography-Mass Spectrometry (GC-MS) Sample Preparation and Analysis

$CD3^+$ T cells isolated from WT mice were activated for 36 hrs before being collected and re-seeded at the density of 2×10^6 cells /mL in conditional media (glucose and glutamine free RPMI-1640, 10%DFBS) containing 10 mM $^{13}C_6$-glucose + 4 mM glutamine or 4 mM $^{13}C_5$-glutamine + 10 mM

glucose. After 0.5, 2, 6, 12 h, around ($\sim1\times10^7$) were collected and washed with PBS 3 times before being snap-frozen (**Fig. S1A-C**). Naïve $CD4^+$ T cells from WT and SDHB cKO were collected and snap-frozen (**Fig. S12A**).

GC-MS was performed as previously described(*77*), cell pellets were resuspended in 0.45 ml -20 °C methanol/ water (1:1 v/v) containing 20 µM L-norvaline as internal standard. Further extraction was performed by adding 0.225 ml chloroform, vortexing, and centrifugation at 15,000×g for 5 min at 4 °C. The upper aqueous phase was evaporated under vacuum using a Speedvac centrifugal evaporator. Separate tubes containing varying amounts of standards were evaporated. Dried samples and standards were dissolved in 30 µl 20 mg/ml isobutylhydroxylamine hydrochloride (TCI #I0387) in pyridine and incubated for 20 min at 80°C. An equal volume of N-tertbutyldimethylsilyl-N-methyltrifluoroacetamide (MTBSTFA) (Soltec Ventures) was added and incubated for 60 min at 80 °C. After derivatization, samples and standards were analyzed by GC-MS using an Rxi-5ms column (15 m x 0.25 i.d. x 0.25 µm, Restek) installed in a Shimadzu QP-2010 Plus gas chromatograph-mass spectrometer (GC-MS). The GC-MS was programmed with an injection temperature of 250°C, 1.0 µl injection volume, and a split ratio of 1/10. The GC oven temperature was initially 130°C for 4 min, rising to 250°C at 6°C/min, and to 280°C at 60°C/min with a final hold at this temperature for 2 min. GC flow rate, with helium as the carrier gas, was 50 cm/s. The GC-MS interface temperature was 300°C, and (electron impact) ion source temperature was 200°C, with 70 eV ionization voltage.

Fractional labeling from ^{13}C substrates and mass isotopomer distributions were calculated as described (*77*). Data from standards were used to construct standard curves in MetaQuant (*78*), from which metabolite amounts in samples were calculated. Metabolite amounts were corrected for recovery of the internal standard and for ^{13}C labeling to yield total (labeled and unlabeled) quantities in nmol per sample and then adjusted per cell number.

Capillary electrophoresis–triple quadrupole/time-of-flight mass spectrometry (CE-QqQ/TOFMS) analysis

$CD3^+$ T cells (around ~1 $\times 10^7$ per sample) isolated from WT and *SDHB* cKO mice were activated for 30 hrs (**Fig. 2G**). T cells were collected by centrifugation (300 ×*g* at 4ºC for 5 min), washed twice with 5% mannitol solution (10 mL first and then 2 mL), then treated with 800 µL of methanol and vortexed for 30 sec to inactivate enzymes. The cell extract was treated with 550 µL of Milli-Q water containing internal standards (H3304-1002, Human Metabolome Technologies, inc., Tsuruoka, Japan) and vortexed for 30 sec. The extract was obtained and centrifuged at 2,300 ×*g* and 4ºC for 5 min, and then 700 µL of the upper aqueous layer was centrifugally filtered through a Millipore 5-kDa cutoff filter at 9,100 ×*g* and 4ºC for 180 min to remove proteins. For CE-MS analysis, the filtrate was centrifugally concentrated and resuspended in 50 µL of Milli-Q water. Cationic compounds were measured in the positive mode of CE-TOFMS, and anionic compounds were measured in the positive and negative modes of CE-MS/MS. Peaks detected by CE-TOFMS and CE-MS/MS were extracted using an automatic integration software (MasterHands, Keio University, Tsuruoka, Japan and MassHunter Quantitative Analysis B.04.00, Agilent Technologies, Santa Clara, CA, USA, respectively) to obtain peak information, including *m/z*, migration time (MT), and peak area. The peaks were annotated with putative metabolites

from the HMT metabolite database based on their MTs in CE and *m/z* values determined by TOFMS. The tolerance range for the peak annotation was configured at ±0.5 min for MT and ±10 ppm for *m/z*. In addition, concentrations of metabolites were calculated by normalizing the peak area of each metabolite with respect to the area of the internal standard and by using standard curves, which were obtained by three-point calibrations.

Metabolite extraction and analysis by ion chromatography-ultra high resolution-Fourier transform mass spectrometry (IC-UHR-FTMS)

$CD3^+$ T Cells (**Fig. 2E and S8B**) were cultured in conditional media (glutamine-free RPMI-1640, 10%DFBS) containing 2 mM $^{13}C_5$-Glutamine for 30 h. ~1 $\times 10^7$ cells for each sample were collected and washed 3 times with cold PBS before being snap-frozen. Naïve $CD4^+$ T cells were polarized under T_H0, T_H1, T_H17, and iT_{reg} culture for 72 h (**Fig. S8E**). Cells were collected and washed with cold PBS 3 times before snap freezing. The frozen cell pellets were homogenized in 60% cold CH3CN in a ball mill (Precellys- 24, Bertin Technologies) for denaturing proteins and optimizing extraction. Polar metabolites were extracted by the solvent partitioning method with a final CH3CN:H2O:CHCl3 (2:1.5:1, v/v) ratio, as described previously(*79*). The polar extracts were reconstituted in nanopure water before analysis on a Dionex ICS-5000+ ion chromatography system interfaced with a Thermo Fusion Orbitrap Tribrid mass spectrometer (Thermo Fisher Scientific) as previously described(*80*) using a *m/z* scan range of 80-700. Peak areas were integrated and exported to Excel via the Thermo TraceFinder (version 3.3) software package before natural abundance correction (*81*). The isotopologue distributions of metabolites were calculated as the mole fractions as previously described (*82*). The number of moles of each metabolite was determined by calibrating the natural abundance-corrected signal against

authentic external standards. The amount was normalized to the amount of extracted protein and is reported in nmol/mg protein.

Succinate and α-KG quantification

CD4+ T cells were treated with 100μM NV118 or 10mM α-KG in a naive condition for 24 h (**Fig.S8C**). Cells were collected for quantifying succinate and α-KG using the succinate colorimetric assay kit (Abcam, ab204718) or α-KG assay kit (Abcam, ab83431). The optical density (OD) values were measured at 450 nm and 570 nm with a Synergy 2 microplate reader (BioTek).

LEGENDplex™ Bead-Based Immunoassay

The supernatants from 36 hrs activated CD4+ T cells were collected for quantifying cytokines using LEGENDplex™ Mouse Th Cytokine Panel (13-plex) V02 kit (Cat. No 740741-V-bottom, Bio Legend, San Diego, USA). The data were collected by Novocyte (ACEA Biosciences) and analyzed using LEGENDplex™ Data Analysis Software V8.0 (BioLegend).

RNA-seq analysis

For RNA sequencing analysis, total RNA was extracted using RNeasy Mini Kit (Qiagen) and treated with DNase I according to the manufacturer's instructions. After assessing the quality of total RNA using an Agilent 2100 Bioanalyzer and RNA Nanochip (Agilent Technologies), 150 ng total RNA was treated to deplete the levels of ribosomal RNA (rRNA) using target-specific oligos combined with rRNA removal beads. Following rRNA removal, mRNA was fragmented and converted into double-stranded cDNA. Adaptor-ligated cDNA was amplified by

limit cycle PCR. After library quality was determined via Agilent 4200 TapeStation and quantified by KAPA qPCR, approximately 60 million paired-end 150 bp sequence reads were generated on the Illumina HiSeq 4000 platform. Quality control and adapter trimming were accomplished using the FastQC (version 0.11.3) and Trim Galore (version 0.4.0) software packages. Trimmed reads were mapped to the Genome Reference Consortium GRCm38 (mm10) murine genome assembly using TopHat2 (version 2.1.0), and feature counts were generated using HTSeq (version 0.6.1). Statistical analysis for differential expression was performed using the DESeq2 package (version 1.16.1) in R, with the default Benjamini-Hochberg *p-value* adjustment method. The Ingenuity Pathway Analysis (IPA) software (QIAGEN), the Gene Set Enrichment Analysis (GSEA) software (UC San Diego, BROAD Ins.), and the R Programming Language software were used to analyze gene signature and pathway enrichment.

ATAC-seq analysis

ATAC-seq was performed as previously described (*83*) with only minor modifications. 5×10^4 cells per experiment were first washed with RSB buffer (10 mM Tris-HCl pH 8, 10 mM NaCl, 3 mM $MgCl_2$) and gently permeabilized with RSB lysis buffer (10 mM Tris-HCl pH 8, 10 mM NaCl, 3 mM $MgCl_2$, 0.1% NP-40) on ice. Cells were suspended in 50 µL of tagmentation master mix prepared from Illumina Tagment DNA TDE1 Enzyme and Buffer Kit components (#20034197), and transposition was performed for 30 minutes at 37°C. Tagmented DNA fragments were isolated using Qiagen MinElute PCR Purification columns prior to library amplification. ATAC-seq libraries were amplified with barcoded Nextera primers for 14 cycles, and excess primers were removed by size selection with AMPure XP beads. Libraries were sequenced on the HiSeq4000 platform running in PEx150bp mode. The ENCODE ATAC-seq

pipeline (https://github.com/ENCODE-DCC/atac-seq-pipeline) with default parameters was used to process ATAC-seq data. First, reads are scanned for adaptor sequences and trimmed with cutadapt (version 2.3). Reads are then mapped to mm10 with bowtie2 (version 2.3.4.3). Properly aligned, non-mitochondrial read pairs were retained for peak calling with MACS2 (version 2.2.4). Differential ATAC peak analysis was completed using DiffBind (Bioconductor) and DESeq2 with an FDR < 0.05. Once differential peaks were called, heatmaps were generated with deeptools (version 3.3.1)(*84*), motif analysis was performed using HOMER (version 4.11.1)(*85*), and nearby genes were identified using GREAT (*86*).

CHIP-qPCR

ChIP was performed as described previously(*87*). Briefly, ~10^7 cells were cross-linked with 1% methanol-free formaldehyde for 10 min at room temperature. The fixation was quenched by adding glycine to a final concentration of 125 mM and placed on ice for 5 minutes. Fixed cells were pelleted at 1,200 × g for 5 minutes at 4°C and resuspended in ice-cold PBS containing a protease inhibitor cocktail. Samples were sonicated with an Active Motif EpiShear probe sonicator. After sonication, a 5µL volume was aliquoted from each sample (input) and combined with 20µL TE, 1µL 10% SDS, and 1µL 20 mg/mL Proteinase K for overnight decrosslinking at 65°C. Input samples were purified using Qiagen MinElute PCR Purification columns, and chromatin fragmentation was assessed by gel electrophoresis on an E-Gel 2% EX agarose gel. The cleared chromatin solutions were immunoprecipitated with antibodies against H3K4me3 (ab8580; Abcam). The normal rabbit IgG (ab171870; Abcam) was used as a background control. Immunoprecipitated complexes were isolated with protein A Dynabeads. ChIP DNA was purified with Qiagen MinElute PCR Purification columns. The DNA was used for ChIP-qPCR

with specific *Prdm1* PCR primers (supplemental Table 5). BIO-RAD CFX96™ Real-Time PCR Detection System was used for SYBR green-based quantitative PCR. The data are presented as fold enrichment over the input control.

CRISPR-Cas 9

All guide RNAs, Alt-R S.p. HIFI Cas9 Nuclease V3, and Alt-R S.p. HIFI electroporation enhancer were purchased from IDT. Mixed 60 pmol of Cas9 protein with 150 pmol of sgRNA and incubated for 20 minutes at room temperature for Cas9/RNP complex formation. Then, activated $CD4^+$ T cells were resuspended in P4 Primary Cell buffer (Lonza) and mixed with the RNP complexes and 4 μM Electroporation Enhancer in P4 Primary Cell buffer (Lonza), transferred the cell/CRISPR mixture to the bottom hole of the wells of the Lonza nucleofector strip for electroporation by using Lonza nucleofector (Program CM137), electroporated cells were recovered in T cell culture medium for 2 h prior to activation with anti-CD3/CD28 antibodies, or under T_H1 or T_H17 polarization. Duplexes of two separate guides per target gene were used: Mm.Cas9.*Prdm1*.1AA (ACACGCTTTGGACCCCTCAT), Mm.Cas9.*Prdm1*.1AB (CATAGTGAACGACCACCCCT).

Statistical analysis

Statistical analysis was conducted using the GraphPad Prism software (GraphPad Software, Inc.). Unpaired two-tail Student's t-test, multiple comparisons of one/ two-way ANOVA were used to assess differences in other experiments. *P* values smaller than 0.05 were considered significant, with $p < 0.05$, $p < 0.01$, $p < 0.001$, and $p < 0.0001$ indicated as *, **, ***, and ****, respectively.

=

Reference and notes

1. L. A. Sena, S. Li, A. Jairaman, M. Prakriya, T. Ezponda, D. A. Hildeman, C. R. Wang, P. T. Schumacker, J. D. Licht, H. Perlman, P. J. Bryce, N. S. Chandel, Mitochondria are required for antigen-specific T cell activation through reactive oxygen species signaling. *Immunity* **38**, 225-236 (2013).
2. V. A. Gerriets, J. C. Rathmell, Metabolic pathways in T cell fate and function. *Trends Immunol* **33**, 168-173 (2012).
3. E. L. Pearce, E. J. Pearce, Metabolic pathways in immune cell activation and quiescence. *Immunity* **38**, 633-643 (2013).
4. C. V. Dang, MYC, metabolism, cell growth, and tumorigenesis. *Cold Spring Harbor perspectives in medicine* **3**, (2013).
5. N. N. Pavlova, C. B. Thompson, The Emerging Hallmarks of Cancer Metabolism. *Cell Metab* **23**, 27-47 (2016).
6. R. E. Gate, C. S. Cheng, A. P. Aiden, A. Siba, M. Tabaka, D. Lituiev, I. Machol, M. G. Gordon, M. Subramaniam, M. Shamim, K. L. Hougen, I. Wortman, S. C. Huang, N. C. Durand, T. Feng, P. L. De Jager, H. Y. Chang, E. L. Aiden, C. Benoist, M. A. Beer, C. J. Ye, A. Regev, Genetic determinants of co-accessible chromatin regions in activated T cells across humans. *Nat Genet* **50**, 1140-1150 (2018).
7. D. Calderon, M. L. T. Nguyen, A. Mezger, A. Kathiria, F. Muller, V. Nguyen, N. Lescano, B. Wu, J. Trombetta, J. V. Ribado, D. A. Knowles, Z. Gao, F. Blaeschke, A. V. Parent, T. D. Burt, M. S.

Anderson, L. A. Criswell, W. J. Greenleaf, A. Marson, J. K. Pritchard, Landscape of stimulation-responsive chromatin across diverse human immune cells. *Nat Genet* **51**, 1494-1505 (2019).

8. Ivanov, II, K. Atarashi, N. Manel, E. L. Brodie, T. Shima, U. Karaoz, D. Wei, K. C. Goldfarb, C. A. Santee, S. V. Lynch, T. Tanoue, A. Imaoka, K. Itoh, K. Takeda, Y. Umesaki, K. Honda, D. R. Littman, Induction of intestinal Th17 cells by segmented filamentous bacteria. *Cell* **139**, 485-498 (2009).
9. C. B. Wilson, E. Rowell, M. Sekimata, Epigenetic control of T-helper-cell differentiation. *Nat Rev Immunol* **9**, 91-105 (2009).
10. K. J. Oestreich, A. S. Weinmann, Encoding stability versus flexibility: lessons learned from examining epigenetics in T helper cell differentiation. *Curr Top Microbiol Immunol* **356**, 145-164 (2012).
11. O. E. Owen, S. C. Kalhan, R. W. Hanson, The key role of anaplerosis and cataplerosis for citric acid cycle function. *J Biol Chem* **277**, 30409-30412 (2002).
12. I. Martinez-Reyes, N. S. Chandel, Mitochondrial TCA cycle metabolites control physiology and disease. *Nat Commun* **11**, 102 (2020).
13. M. P. Murphy, L. A. J. O'Neill, Krebs Cycle Reimagined: The Emerging Roles of Succinate and Itaconate as Signal Transducers. *Cell* **174**, 780-784 (2018).
14. M. Xiao, H. Yang, W. Xu, S. Ma, H. Lin, H. Zhu, L. Liu, Y. Liu, C. Yang, Y. Xu, S. Zhao, D. Ye, Y. Xiong, K. L. Guan, Inhibition of alpha-KG-dependent histone and DNA demethylases by fumarate and succinate that are accumulated in mutations of FH and SDH tumor suppressors. *Genes Dev* **26**, 1326-1338 (2012).
15. L. J. Walport, R. J. Hopkinson, C. J. Schofield, Mechanisms of human histone and nucleic acid demethylases. *Curr Opin Chem Biol* **16**, 525-534 (2012).

16. J. A. van der Knaap, C. P. Verrijzer, Undercover: gene control by metabolites and metabolic enzymes. *Genes Dev* **30**, 2345-2369 (2016).

17. Y. Tsukada, J. Fang, H. Erdjument-Bromage, M. E. Warren, C. H. Borchers, P. Tempst, Y. Zhang, Histone demethylation by a family of JmjC domain-containing proteins. *Nature* **439**, 811-816 (2006).

18. E. Gottlieb, I. P. Tomlinson, Mitochondrial tumour suppressors: a genetic and biochemical update. *Nat Rev Cancer* **5**, 857-866 (2005).

19. A. King, M. A. Selak, E. Gottlieb, Succinate dehydrogenase and fumarate hydratase: linking mitochondrial dysfunction and cancer. *Oncogene* **25**, 4675-4682 (2006).

20. G. Andrejeva, J. C. Rathmell, Similarities and Distinctions of Cancer and Immune Metabolism in Inflammation and Tumors. *Cell Metab* **26**, 49-70 (2017).

21. W. Bailis, J. A. Shyer, J. Zhao, J. C. G. Canaveras, F. J. Al Khazal, R. Qu, H. R. Steach, P. Bielecki, O. Khan, R. Jackson, Y. Kluger, L. J. Maher, 3rd, J. Rabinowitz, J. Craft, R. A. Flavell, Distinct modes of mitochondrial metabolism uncouple T cell differentiation and function. *Nature* **571**, 403-407 (2019).

22. J. K. Ehinger, S. Piel, R. Ford, M. Karlsson, F. Sjovall, E. A. Frostner, S. Morota, R. W. Taylor, D. M. Turnbull, C. Cornell, S. J. Moss, C. Metzsch, M. J. Hansson, H. Fliri, E. Elmer, Cell-permeable succinate prodrugs bypass mitochondrial complex I deficiency. *Nat Commun* **7**, 12317 (2016).

23. H. Miyadera, K. Shiomi, H. Ui, Y. Yamaguchi, R. Masuma, H. Tomoda, H. Miyoshi, A. Osanai, K. Kita, S. Omura, Atpenins, potent and specific inhibitors of mitochondrial complex II (succinate-ubiquinone oxidoreductase). *Proceedings of the National Academy of Sciences of the United States of America* **100**, 473-477 (2003).

24. R. Wang, C. P. Dillon, L. Z. Shi, S. Milasta, R. Carter, D. Finkelstein, L. L. McCormick, P. Fitzgerald, H. Chi, J. Munger, D. R. Green, The transcription factor Myc controls metabolic reprogramming upon T lymphocyte activation. *Immunity* **35**, 871-882 (2011).

25. C. K. Mathews, Deoxyribonucleotide metabolism, mutagenesis and cancer. *Nat Rev Cancer* **15**, 528-539 (2015).

26. C. L. Quinlan, A. L. Orr, I. V. Perevoshchikova, J. R. Treberg, B. A. Ackrell, M. D. Brand, Mitochondrial complex II can generate reactive oxygen species at high rates in both the forward and reverse reactions. *J Biol Chem* **287**, 27255-27264 (2012).

27. B. Diaz-Castro, C. O. Pintado, P. Garcia-Flores, J. Lopez-Barneo, J. I. Piruat, Differential impairment of catecholaminergic cell maturation and survival by genetic mitochondrial complex II dysfunction. *Mol Cell Biol* **32**, 3347-3357 (2012).

28. H. K. Eltzschig, P. Carmeliet, Hypoxia and inflammation. *N Engl J Med* **364**, 656-665 (2011).

29. A. Palazon, A. W. Goldrath, V. Nizet, R. S. Johnson, HIF transcription factors, inflammation, and immunity. *Immunity* **41**, 518-528 (2014).

30. S. Raghuraman, I. Donkin, S. Versteyhe, R. Barres, D. Simar, The Emerging Role of Epigenetics in Inflammation and Immunometabolism. *Trends Endocrinol Metab* **27**, 782-795 (2016).

31. W. Xu, H. Yang, Y. Liu, Y. Yang, P. Wang, S. H. Kim, S. Ito, C. Yang, P. Wang, M. T. Xiao, L. X. Liu, W. Q. Jiang, J. Liu, J. Y. Zhang, B. Wang, S. Frye, Y. Zhang, Y. H. Xu, Q. Y. Lei, K. L. Guan, S. M. Zhao, Y. Xiong, Oncometabolite 2-hydroxyglutarate is a competitive inhibitor of alpha-ketoglutarate-dependent dioxygenases. *Cancer Cell* **19**, 17-30 (2011).

32. J. J. Bird, D. R. Brown, A. C. Mullen, N. H. Moskowitz, M. A. Mahowald, J. R. Sider, T. F. Gajewski, C. R. Wang, S. L. Reiner, Helper T cell differentiation is controlled by the cell cycle. *Immunity* **9**, 229-237 (1998).

33. C. Yang, J. C. Matro, K. M. Huntoon, D. Y. Ye, T. T. Huynh, S. M. Fliedner, J. Breza, Z. Zhuang, K. Pacak, Missense mutations in the human SDHB gene increase protein degradation without altering intrinsic enzymatic function. *FASEB J* **26**, 4506-4516 (2012).

34. P. Lee, N. S. Chandel, M. C. Simon, Cellular adaptation to hypoxia through hypoxia inducible factors and beyond. *Nat Rev Mol Cell Biol* **21**, 268-283 (2020).

35. G. L. Semenza, Hypoxia-inducible factors in physiology and medicine. *Cell* **148**, 399-408 (2012).

36. G. M. Tannahill, A. M. Curtis, J. Adamik, E. M. Palsson-McDermott, A. F. McGettrick, G. Goel, C. Frezza, N. J. Bernard, B. Kelly, N. H. Foley, L. Zheng, A. Gardet, Z. Tong, S. S. Jany, S. C. Corr, M. Haneklaus, B. E. Caffrey, K. Pierce, S. Walmsley, F. C. Beasley, E. Cummins, V. Nizet, M. Whyte, C. T. Taylor, H. Lin, S. L. Masters, E. Gottlieb, V. P. Kelly, C. Clish, P. E. Auron, R. J. Xavier, L. A. O'Neill, Succinate is an inflammatory signal that induces IL-1beta through HIF-1alpha. *Nature* **496**, 238-242 (2013).

37. E. V. Dang, J. Barbi, H. Y. Yang, D. Jinasena, H. Yu, Y. Zheng, Z. Bordman, J. Fu, Y. Kim, H. R. Yen, W. Luo, K. Zeller, L. Shimoda, S. L. Topalian, G. L. Semenza, C. V. Dang, D. M. Pardoll, F. Pan, Control of T(H)17/T(reg) balance by hypoxia-inducible factor 1. *Cell* **146**, 772-784 (2011).

38. L. Liu, Y. Lu, J. Martinez, Y. Bi, G. Lian, T. Wang, S. Milasta, J. Wang, M. Yang, G. Liu, D. R. Green, R. Wang, Proinflammatory signal suppresses proliferation and shifts macrophage metabolism from Myc-dependent to HIF1alpha-dependent. *Proceedings of the National Academy of Sciences of the United States of America* **113**, 1564-1569 (2016).

39. T. Kouzarides, Chromatin modifications and their function. *Cell* **128**, 693-705 (2007).

40. X. Wu, Y. Zhang, TET-mediated active DNA demethylation: mechanism, function and beyond. *Nat Rev Genet* **18**, 517-534 (2017).

41. S. L. Gaffen, R. Jain, A. V. Garg, D. J. Cua, The IL-23-IL-17 immune axis: from mechanisms to therapeutic testing. *Nat Rev Immunol* **14**, 585-600 (2014).

42. R. Jain, Y. Chen, Y. Kanno, B. Joyce-Shaikh, G. Vahedi, K. Hirahara, W. M. Blumenschein, S. Sukumar, C. J. Haines, S. Sadekova, T. K. McClanahan, M. J. McGeachy, J. J. O'Shea, D. J. Cua, Interleukin-23-Induced Transcription Factor Blimp-1 Promotes Pathogenicity of T Helper 17 Cells. *Immunity* **44**, 131-142 (2016).

43. T. E. Beach, H. A. Prag, L. Pala, A. Logan, M. M. Huang, A. V. Gruszczyk, J. L. Martin, K. Mahbubani, M. O. Hamed, S. A. Hosgood, M. L. Nicholson, A. M. James, R. C. Hartley, M. P. Murphy, K. Saeb-Parsy, Targeting succinate dehydrogenase with malonate ester prodrugs decreases renal ischemia reperfusion injury. *Redox Biol* **36**, 101640 (2020).

44. C. Johansson, A. Tumber, K. Che, P. Cain, R. Nowak, C. Gileadi, U. Oppermann, The roles of Jumonji-type oxygenases in human disease. *Epigenomics* **6**, 89-120 (2014).

45. Y. Dou, T. A. Milne, A. J. Tackett, E. R. Smith, A. Fukuda, J. Wysocka, C. D. Allis, B. T. Chait, J. L. Hess, R. G. Roeder, Physical association and coordinate function of the H3 K4 methyltransferase MLL1 and the H4 K16 acetyltransferase MOF. *Cell* **121**, 873-885 (2005).

46. C. Johansson, S. Velupillai, A. Tumber, A. Szykowska, E. S. Hookway, R. P. Nowak, C. Strain-Damerell, C. Gileadi, M. Philpott, N. Burgess-Brown, N. Wu, J. Kopec, A. Nuzzi, H. Steuber, U. Egner, V. Badock, S. Munro, N. B. LaThangue, S. Westaway, J. Brown, N. Athanasou, R. Prinjha, P. E. Brennan, U. Oppermann, Structural analysis of human KDM5B guides histone demethylase inhibitor development. *Nature chemical biology* **12**, 539-545 (2016).

47. H. Karatas, E. C. Townsend, F. Cao, Y. Chen, D. Bernard, L. Liu, M. Lei, Y. Dou, S. Wang, High-affinity, small-molecule peptidomimetic inhibitors of MLL1/WDR5 protein-protein interaction. *J Am Chem Soc* **135**, 669-682 (2013).

48. S. Weis, A. R. Carlos, M. R. Moita, S. Singh, B. Blankenhaus, S. Cardoso, R. Larsen, S. Rebelo, S. Schauble, L. Del Barrio, G. Mithieux, F. Rajas, S. Lindig, M. Bauer, M. P. Soares, Metabolic Adaptation Establishes Disease Tolerance to Sepsis. *Cell* **169**, 1263-1275 e1214 (2017).

49. E. D. Weinberg, Nutritional immunity. Host's attempt to withold iron from microbial invaders. *JAMA* **231**, 39-41 (1975).

50. M. Slack, T. Wang, R. Wang, T cell metabolic reprogramming and plasticity. *Molecular immunology* **68**, 507-512 (2015).

51. K. Troha, J. S. Ayres, Metabolic Adaptations to Infections at the Organismal Level. *Trends Immunol* **41**, 113-125 (2020).

52. H. Chi, Regulation and function of mTOR signalling in T cell fate decisions. *Nature Reviews Immunology* **12**, 325-338 (2012).

53. J. D. Powell, G. M. Delgoffe, The mammalian target of rapamycin: linking T cell differentiation, function, and metabolism. *Immunity* **33**, 301-311 (2010).

54. R. D. Michalek, J. C. Rathmell, The metabolic life and times of a T-cell. *Immunol Rev* **236**, 190-202 (2010).

55. K. Birsoy, T. Wang, W. W. Chen, E. Freinkman, M. Abu-Remaileh, D. M. Sabatini, An Essential Role of the Mitochondrial Electron Transport Chain in Cell Proliferation Is to Enable Aspartate Synthesis. *Cell* **162**, 540-551 (2015).

56. A. T. Phan, A. W. Goldrath, C. K. Glass, Metabolic and Epigenetic Coordination of T Cell and Macrophage Immunity. *Immunity* **46**, 714-729 (2017).

57. B. E. Russ, J. E. Prier, S. Rao, S. J. Turner, T cell immunity as a tool for studying epigenetic regulation of cellular differentiation. *Front Genet* **4**, 218 (2013).

58. L. B. Sullivan, D. Y. Gui, A. M. Hosios, L. N. Bush, E. Freinkman, M. G. Vander Heiden, Supporting Aspartate Biosynthesis Is an Essential Function of Respiration in Proliferating Cells. *Cell* **162**, 552-563 (2015).

59. D. Y. Gui, L. B. Sullivan, A. Luengo, A. M. Hosios, L. N. Bush, N. Gitego, S. M. Davidson, E. Freinkman, C. J. Thomas, M. G. Vander Heiden, Environment Dictates Dependence on Mitochondrial Complex I for NAD+ and Aspartate Production and Determines Cancer Cell Sensitivity to Metformin. *Cell Metab* **24**, 716-727 (2016).

60. E. Gaude, C. Schmidt, P. A. Gammage, A. Dugourd, T. Blacker, S. P. Chew, J. Saez-Rodriguez, J. S. O'Neill, G. Szabadkai, M. Minczuk, C. Frezza, NADH Shuttling Couples Cytosolic Reductive Carboxylation of Glutamine with Glycolysis in Cells with Mitochondrial Dysfunction. *Mol Cell* **69**, 581-593 e587 (2018).

61. S. Cardaci, L. Zheng, G. MacKay, N. J. van den Broek, E. D. MacKenzie, C. Nixon, D. Stevenson, S. Tumanov, V. Bulusu, J. J. Kamphorst, A. Vazquez, S. Fleming, F. Schiavi, G. Kalna, K. Blyth, D. Strathdee, E. Gottlieb, Pyruvate carboxylation enables growth of SDH-deficient cells by supporting aspartate biosynthesis. *Nat Cell Biol* **17**, 1317-1326 (2015).

62. C. Lussey-Lepoutre, K. E. Hollinshead, C. Ludwig, M. Menara, A. Morin, L. J. Castro-Vega, S. J. Parker, M. Janin, C. Martinelli, C. Ottolenghi, C. Metallo, A. P. Gimenez-Roqueplo, J. Favier, D. A. Tennant, Loss of succinate dehydrogenase activity results in dependency on pyruvate carboxylation for cellular anabolism. *Nat Commun* **6**, 8784 (2015).

63. E. L. Mills, B. Kelly, A. Logan, A. S. H. Costa, M. Varma, C. E. Bryant, P. Tourlomousis, J. H. M. Dabritz, E. Gottlieb, I. Latorre, S. C. Corr, G. McManus, D. Ryan, H. T. Jacobs, M. Szibor, R. J. Xavier, T. Braun, C. Frezza, M. P. Murphy, L. A. O'Neill, Succinate Dehydrogenase Supports

Metabolic Repurposing of Mitochondria to Drive Inflammatory Macrophages. *Cell* **167**, 457-470 e413 (2016).

64. C. Nastasi, A. Willerlev-Olsen, K. Dalhoff, S. L. Ford, A. O. Gadsboll, T. B. Buus, M. Gluud, M. Danielsen, T. Litman, C. M. Bonefeld, C. Geisler, N. Odum, A. Woetmann, Inhibition of succinate dehydrogenase activity impairs human T cell activation and function. *Sci Rep* **11**, 1458 (2021).

65. E. Mills, L. A. O'Neill, Succinate: a metabolic signal in inflammation. *Trends Cell Biol* **24**, 313-320 (2014).

66. M. N. Artyomov, A. Sergushichev, J. D. Schilling, Integrating immunometabolism and macrophage diversity. *Semin Immunol* **28**, 417-424 (2016).

67. V. Lampropoulou, A. Sergushichev, M. Bambouskova, S. Nair, E. E. Vincent, E. Loginicheva, L. Cervantes-Barragan, X. Ma, S. C. Huang, T. Griss, C. J. Weinheimer, S. Khader, G. J. Randolph, E. J. Pearce, R. G. Jones, A. Diwan, M. S. Diamond, M. N. Artyomov, Itaconate Links Inhibition of Succinate Dehydrogenase with Macrophage Metabolic Remodeling and Regulation of Inflammation. *Cell Metab* **24**, 158-166 (2016).

68. A. Swain, M. Bambouskova, H. Kim, P. S. Andhey, D. Duncan, K. Auclair, V. Chubukov, D. M. Simons, T. P. Roddy, K. M. Stewart, M. N. Artyomov, Comparative evaluation of itaconate and its derivatives reveals divergent inflammasome and type I interferon regulation in macrophages. *Nat Metab* **2**, 594-602 (2020).

69. W. He, F. J. Miao, D. C. Lin, R. T. Schwandner, Z. Wang, J. Gao, J. L. Chen, H. Tian, L. Ling, Citric acid cycle intermediates as ligands for orphan G-protein-coupled receptors. *Nature* **429**, 188-193 (2004).

70. D. G. Ryan, M. P. Murphy, C. Frezza, H. A. Prag, E. T. Chouchani, L. A. O'Neill, E. L. Mills, Coupling Krebs cycle metabolites to signalling in immunity and cancer. *Nat Metab* **1**, 16-33 (2019).

71. S. E. Weinberg, B. D. Singer, E. M. Steinert, C. A. Martinez, M. M. Mehta, I. Martinez-Reyes, P. Gao, K. A. Helmin, H. Abdala-Valencia, L. A. Sena, P. T. Schumacker, L. A. Turka, N. S. Chandel, Mitochondrial complex III is essential for suppressive function of regulatory T cells. *Nature* **565**, 495-499 (2019).

72. W. C. Skarnes, B. Rosen, A. P. West, M. Koutsourakis, W. Bushell, V. Iyer, A. O. Mujica, M. Thomas, J. Harrow, T. Cox, D. Jackson, J. Severin, P. Biggs, J. Fu, M. Nefedov, P. J. de Jong, A. F. Stewart, A. Bradley, A conditional knockout resource for the genome-wide study of mouse gene function. *Nature* **474**, 337-342 (2011).

73. H. E. Ryan, M. Poloni, W. McNulty, D. Elson, M. Gassmann, J. M. Arbeit, R. S. Johnson, Hypoxia-inducible factor-1alpha is a positive factor in solid tumor growth. *Cancer Res* **60**, 4010-4015 (2000).

74. M. Habib, F. Fares, C. A. Bourgeois, C. Bella, J. Bernardino, F. Hernandez-Blazquez, A. de Capoa, A. Niveleau, DNA global hypomethylation in EBV-transformed interphase nuclei. *Exp Cell Res* **249**, 46-53 (1999).

75. X. Chen, J. W. Sherman, R. Wang, Radioisotope-Based Protocol for Determination of Central Carbon Metabolism in T Cells. *Methods Mol Biol* **2111**, 257-265 (2020).

76. L. Z. Shi, R. Wang, G. Huang, P. Vogel, G. Neale, D. R. Green, H. Chi, HIF1alpha-dependent glycolytic pathway orchestrates a metabolic checkpoint for the differentiation of TH17 and Treg cells. *J Exp Med* **208**, 1367-1376 (2011).

77. B. Ratnikov, P. Aza-Blanc, Z. A. Ronai, J. W. Smith, A. L. Osterman, D. A. Scott, Glutamate and asparagine cataplerosis underlie glutamine addiction in melanoma. *Oncotarget* **6**, 7379-7389 (2015).

78. B. Bunk, M. Kucklick, R. Jonas, R. Munch, M. Schobert, D. Jahn, K. Hiller, MetaQuant: a tool for the automatic quantification of GC/MS-based metabolome data. *Bioinformatics* **22**, 2962-2965 (2006).

79. F. T.WM, Considerations of Sample Preparation for Metabolomics Investigation. In: Fan TM., Lane A., Higashi R. (eds) The Handbook of Metabolomics. *Methods in Pharmacology and Toxicology*, (2012).

80. T. W. Fan, M. O. Warmoes, Q. Sun, H. Song, J. Turchan-Cholewo, J. T. Martin, A. Mahan, R. M. Higashi, A. N. Lane, Distinctly perturbed metabolic networks underlie differential tumor tissue damages induced by immune modulator beta-glucan in a two-case ex vivo non-small-cell lung cancer study. *Cold Spring Harb Mol Case Stud* **2**, a000893 (2016).

81. H. N. Moseley, Correcting for the effects of natural abundance in stable isotope resolved metabolomics experiments involving ultra-high resolution mass spectrometry. *BMC Bioinformatics* **11**, 139 (2010).

82. A. N. Lane, T. W. Fan, R. M. Higashi, Isotopomer-based metabolomic analysis by NMR and mass spectrometry. *Methods Cell Biol* **84**, 541-588 (2008).

83. J. D. Buenrostro, P. G. Giresi, L. C. Zaba, H. Y. Chang, W. J. Greenleaf, Transposition of native chromatin for fast and sensitive epigenomic profiling of open chromatin, DNA-binding proteins and nucleosome position. *Nat Methods* **10**, 1213-1218 (2013).

84. F. Ramirez, D. P. Ryan, B. Gruning, V. Bhardwaj, F. Kilpert, A. S. Richter, S. Heyne, F. Dundar, T. Manke, deepTools2: a next generation web server for deep-sequencing data analysis. *Nucleic Acids Res* **44**, W160-165 (2016).

85. S. Heinz, C. Benner, N. Spann, E. Bertolino, Y. C. Lin, P. Laslo, J. X. Cheng, C. Murre, H. Singh, C. K. Glass, Simple combinations of lineage-determining transcription factors prime cis-regulatory elements required for macrophage and B cell identities. *Mol Cell* **38**, 576-589 (2010).

86. C. Y. McLean, D. Bristor, M. Hiller, S. L. Clarke, B. T. Schaar, C. B. Lowe, A. M. Wenger, G. Bejerano, GREAT improves functional interpretation of cis-regulatory regions. *Nat Biotechnol* **28**, 495-501 (2010).

87. B. D. Sunkel, M. Wang, S. LaHaye, B. J. Kelly, J. R. Fitch, F. G. Barr, P. White, B. Z. Stanton, Evidence of pioneer factor activity of an oncogenic fusion transcription factor. *iScience* **24**, 102867 (2021).

Acknowledgments

Funding: This work was supported by 1UO1CA232488-01 from the National Institute of Health (Cancer Moonshot program), 2R01AI114581-06, and RO1CA247941 from the National Institute of Health, V2014-001 from the V-Foundation, and 128436-RSG-15-180-01-LIB from the American Cancer Society (to RW). The Sanford Burnham Prebys Cancer Metabolism Core was supported by the SBP NCI Cancer Center Support Grant P30 CA030199. The Center for Environmental and Systems Biochemistry Core was supported by the Markey Cancer Center support grant P30CA177558.

Author contributions: R. Wang conceptualized and supervised this work. X.C. carried out most of the experiments. B.S., B.S., and M.W. performed and analyzed the CD4 T cells ATAC seq and RNA seq data. S.K., T.W., J.R.G., L.L., T.A.C., D.A.S., Y.Y., A.N.L., and G.X. were involved in data collection, analysis, and review. B.S., and T.W.F., provided conceptual input into the study development. A.M.MC. and J.LB provided some experimental animals. X.C., B.S., A.N.L., T.W.F., and R. Wang wrote the manuscript. All authors discussed the results and provided feedback on the manuscript.

Competing interests: All other authors declare no conflict of interest.

Data availability statement: The $CD3^+$ T cells RNA-seq datasets generated for this study can be found in the GEO accession GSE184010. The $CD4^+$ T cells RNA-seq datasets generated for this study can be found in the GEO accession GSE184743. The $CD4^+$ T cells ATAC-seq datasets generated for this study can be found in the GEO accession GSE184742. SDHB-flox mouse strain is available from Dr. Ruoning Wang's laboratory under a material transfer agreement with the Nationwide Children's Hospital. All data needed to evaluate the conclusions in the paper are present in the paper or the Supplementary Materials.

Figure Captions

Figure 1. SDHB is required for the T cell proliferation and survival.

(**A**) SDHB mRNA and protein levels of the indicated T cells were determined by qPCR and Immunoblot (n=3), ***$p < 0.001$, Student's *t* test. **(B)** Metabolites of the indicated T cells were determined by CE-QqQ/TOFMS (n=3), **$p < 0.01$, ***$p < 0.001$, Student's *t* test. **(C)** The cell cycle profile of the indicated $CD4^+$ T cells was analyzed by BrdU and 7AAD staining. The numbers indicate the percentage of cells in the cell cycle stage. (**D**) Cell proliferation of the indicated $CD4^+$ T cells was determined by CFSE dilution. (**E-F**) Cell viability of the indicated $CD4^+$ T cells was assessed by 7AAD uptake, n=3, data are representative of 3 independent experiments, n.s., not significant, ***$p < 0.001$, one-way ANOVA. T cells (B-F) were activated by the plate-bound anti-CD3/CD28 antibodies. (**G**) Diagram of *in vivo* competitive proliferation experimental procedure (top panel). The donor $CD4^+$ T cell ratios before and after adoptive transfer were evaluated by surface staining of isogenic markers, and cell proliferation was evaluated by CFSE dilution (bottle panel). Representative flow plots of the donor T cells were gated from $TCR\beta^+CD4^+$ cells and parsed by Thy1.1(WT) and Thy1.2(*SDHB* cKO). Data represent 3 independent experiments. (**H**) Diagram of *in vivo* antigen-specific competitive proliferation experimental procedure (top panel), the donor $CD4^+$ T cell ratios before and after adoptive transfer were evaluated by surface staining of isogenic markers, and cell proliferation was evaluated by CFSE dilution (bottle panel). Representative flow plots of the donor T cells were gated from $CD45.2^+CD4^+$ cells and parsed by Thy1.1(WT) and Thy1.2(*SDHB* cKO). Data represent of 3 independent experiments. (**I**) Diagram of EAE experimental procedure (left panel), clinical scores were evaluated daily (right panel), n=5 mice for each group, experiments were repeated 3 times. **(J)** H&E staining of spinal cord sections from WT and *SDHB* cKO mice after

EAE induction, leukocyte infiltration are marked by arrowheads. Scale bar, 200μm. Bar graphs, mean ± SEM.

Figure 2. SDHB deficiency decouples the TCA cycle from nucleoside biosynthesis.

(A-D) The catabolic activities of the indicated T cells were measured by the generation of $^{3}H_2O$ from Glucose, D-[5-^{3}H(N)] (**A**), $^{14}CO_2$ from D-Glucose, [1-^{14}C] **(B)**, $^{3}H_2O$ from Palmitic acid, [9,10-^{3}H] (**C**), $^{14}CO_2$ from [U-^{14}C]-glutamine **(D),** n=3, data are representative of 2 independent experiments. n.s., not significant, $^{**}p < 0.01$, $^{***}p < 0.001$, Student's *t* test**. (E)** Diagram of [$^{13}C_5$]-Glutamine catabolism through entering the downstream TCA cycle, aspartate synthesis and pyrimidine biosynthesis. α-KG: α-ketoglutarate; XMP: uridine, cytidine and thymidine monophosphate; SDH: Succinate dehydrogenase; ●: denoted the ^{13}C label of all carbons of indicated metabolites that are derived from [$^{13}C_5$]-glutamine catabolism. Solid and dashed arrows represent single- and multi-step reactions (left panel), metabolites were extracted and analyzed using IC-UHR-FTMS (right panel), numbers in the X-axis represent those of ^{13}C atoms in given metabolites, and numbers in the Y-axis represent the levels of the metabolites (μmole/g protein). n=3 from one experiment, $^{*}p < 0.05$, $^{***}p < 0.001$, two-way ANOVA. UMP/UDP: uridine mono/diphosphate; dUMP deoxyuridine monophosphate; CMP/CDP: uridine mono/diphosphate; dTMP: deoxythymidine monophosphate; **(F)** The incorporation of carbon from ^{14}C-glutamine into DNA and RNA was determined by the isotope uptake, n=3, data are representative of 2 independent experiments. $^{*}p < 0.05$, Student's *t* test. **(G)** Metabolites of the indicated T cells were determined by CE-QqQ/TOFMS and depicted in the Heatmap. **(H)** DNA and RNA content of the indicated $CD4^{+}$ T cells were determined by the 7AAD and pyronin-Y uptake. Bar graphs, mean ± SEM. T cells were activated by the plate-bound anti-CD3/CD28 antibodies.

Figure 3. Nucleoside supplementation partially compensates for the loss of de novo biosynthesis of nucleotides in SDHB cKO T cells.

(A-D) $CD4^+$ T cells were activated for 72 hrs with or without nucleosides (NS: adenosine, guanosine, thymidine, cytidine, uridine and inosine), cell viability was calculated based on the 7AAD staining (**A-B**), cell number was measured by a cell counter (**C**), cell proliferation was determined by CFSE dilution (**D**), n=3, data are representative of 3 independent experiments, $^{**}p < 0.01$, $^{***}p < 0.001$, one-way ANOVA**. (E)** DNA and RNA content of the indicated T cells (plate-bound anti-CD3/CD28 activation for 36 hrs) were determined by the 7AAD and pyronin staining. **(F)** The cell cycle profile of the indicated T cells (plate-bound anti-CD3/CD28 activation for 48 hrs) was analyzed by BrdU and 7AAD staining. **(G-J)** $CD4^+$ T cells were activated for 72 hrs with TCU (thymidine, cytidine and uridine), TCUI (thymidine, cytidine, uridine and inosine), or NS, cell viability was determined by the 7AAD uptake **(G-H)**, and cell number was measured by a cell counter **(I)**, cell proliferation was determined by CFSE dilution **(J)**, n=3, data are representative of 3 independent experiments, $^{*}p < 0.05$, $^{***}p < 0.001$, one-way ANOVA. Bar graphs, mean ± SEM. T cells were activated by the plate-bound anti-CD3/CD28 antibodies.

Figure 4. SDHB deficiency promotes a pro-inflammatory gene signature in T cells after activation.

(A-C) Transcriptomic analysis of RNA-seq data in activated $CD3^+$ T cells (30h). (**A**) Volcano plot. The $\log_2$ FC indicates the mean expression level for each gene. Each dot represents one gene. Red dots represent up-regulated genes; black dots represent down-regulated genes; the blue

dots indicate presentative genes in the hallmark gene sets. Highlighted genes (**A**) were selected based on genes of interest. **(B)** The most up-regulated pathways were identified by ingenuity pathway analysis (IPA). **(C)** The signature of differentially expressed genes was identified by GSEA. **(D)** mRNA levels of indicated genes were determined by qPCR, n=3, data are representative of 3 independent experiments, $*p < 0.05$, $***p < 0.001$, one-way ANOVA. **(E)** $CD4^+$ T cells were activated for 36 hrs with indicated treatment, mRNA levels of indicated genes were measured by qPCR, n=3, data are representative of 3 independent experiments, n.s., not significant, $***p < 0.001$, one-way ANOVA. **(F)** Cell culture media from the indicated T cell groups (36 hrs after activation) were collected, mixed with fresh medium at 1:1 ratio, and then were used for culturing WT T cells for 36 hrs under activation condition (left panel), mRNA levels of indicated genes were measured by the qPCR (right panel), n=3, data are representative of 2 independent experiments, n.s., not significant, $*p < 0.05$, Student's *t* test. Bar graphs, mean ± SEM. NS: nucleosides. T cells were activated by the plate-bound anti-CD3/CD28 antibodies.

Figure 5. Increasing the intracellular succinate/α-KG ratio promotes pro-inflammatory signature in T cells after activation.

(A) Schematic diagram of succinate-mediated metabolic, signaling, and epigenetic regulation of T cell proliferation and inflammation. **(B)** $CD4^+$ T cells were cultured with 100μM cell permeable succinate (NV118) followed by activation as indicated in the experimental diagram (top panel), mRNA levels of indicated genes were measured by qPCR (bottom panel, n=3, data are representative of 3 independent experiments, $*p < 0.05$, $**p < 0.01$, $***p < 0.001$, student's *t* test**. (C)** $CD4^+$ T cells were activated for 36 hrs with or without 10mM α-KG, mRNA levels of indicated genes were measured by qPCR, n=3, data are representative of 3 independent

experiments, ***p<0.001, one-way ANOVA**. **(D)** Schematic diagram of R162's action and glutamine catabolism (left panel), $CD4^+$ T cells were activated for 36 hrs with indicated treatments, mRNA levels of indicated genes were measured by the qPCR (right panel), n=3, data are representative of 2 independent experiments, ***p < 0.001, one-way ANOVA. T cells (B-D) were activated by the plate-bound anti-CD3/CD28 antibodies. **(E-F)** $CD4^+$ T cells were polarized toward T_H1 **(E)** and T_H17 **(F)** lineages for 72 hrs with indicated treatments (2mM α-KG and 25μM NV118). The indicated proteins were quantified by intracellular staining by flow cytometry. Cell proliferation was determined by CFSE staining, n=3, data are representative of 3 independent experiments, *p<0.05, **p<0.01, ***p<0.001, one-way ANOVA. Bar graphs, mean ± SEM.

Figure 6. SDHB deficiency increases the level of succinate to enhance DNA accessibility and pro-inflammatory genes transcription.

(**A**) Differential chromatin accessibility was measured by ATAC-seq in activated $CD4^+$ T cells between indicated genotypes (n=3 replicates for each genotype), identifying 8,543 sites with accessibility gain and 1,521 sites with accessibility loss in activated *SDHB* cKO T cells. (**B**) ATAC-seq peaks with differential accessibility were linked to nearby genes, and ontology analysis was performed using GREAT. (**C**) Accessibility changes in differential ATAC-seq peaks were plotted against expression changes ($CD4^+$ T cells RNA-seq) in the nearby genes identified in (**B**), concordant changes (i.e., enhanced expression and accessibility) were observed among pro-inflammatory genes and master transcription factors mediating inflammation. (**D**) Motif analysis was performed on ATAC-seq peaks showing enhanced accessibility in activated *SDHB* cKO $CD4^+$ T cells. A volcano plot shows up-regulated expression of many cognate transcription

factors by RNA-seq. Highlighted genes (**C&D**) were selected based on genes of interest. **(E)** mRNA levels of transcription factors in the indicated $CD4^+$ T cells were depicted in the Heatmap, (n=3 replicates for each group). **(F)** $CD4^+$ T cells were activated for 36 hrs with or without 10mM α-KG, Blimp1 protein levels were measured by intracellular staining by flow cytometry, MFI was analyzed, n=3, data are representative of 3 independent experiments, $**p<0.01$, $***p<0.001$, one-way ANOVA. **(G)** $CD4^+$ T cells were maintained in naïve condition with 100μM NV118 for 72 hrs and then activated for 36 h, Blimp1 protein levels were measured by intracellular staining by flow cytometry, MFI was analyzed, n=3, data are representative of 3 independent experiments, $**p<0.01$, student's *t* test. Bar graphs, mean ± SEM. T cells were activated by the plate-bound anti-CD3/CD28 antibodies.

Figure 7. Succinate-mediated *Prdm1*/Blimp1 expression contributes to proinflammatory signature in T cells.

(A) $CD4^+$ T cells were activated overnight, then electroporated with g*Prdm1* and Cas9, cells were recovered in culture medium for 2 hrs prior to activation for 40 hrs (top panel), Blimp-1 protein levels were measured by intracellular staining by flow cytometry (bottle panel), n=3, data are representative of 2 independent experiments, $**p < 0.01$, one-way ANOVA. **(B)** $CD4^+$ T cells were electroporated with g*Prdm1* and Cas9, mRNA levels of indicated genes were determined by qPCR, n=3, data are representative of 2 independent experiments, n.s., not significant, $**p < 0.01$, $***p < 0.001$, one-way ANOVA. **(C-D)** $CD4^+$ T cells were activated overnight, then electroporated with g*Prdm1* and Cas9. Cells were then polarized toward T_H1 **(C)** and T_H17 **(D)** lineages for 72 hrs with or without 25μM NV118. The indicated proteins were quantified by intracellular staining by flow cytometry, cell proliferation was determined by CFSE staining.

n=3, data are representative of 2 independent experiments, ***$p < 0.001$, one-way ANOVA. Bar graphs, mean ± SEM. T cells were activated by the plate-bound anti-CD3/CD28 antibodies.

"Figure #1"

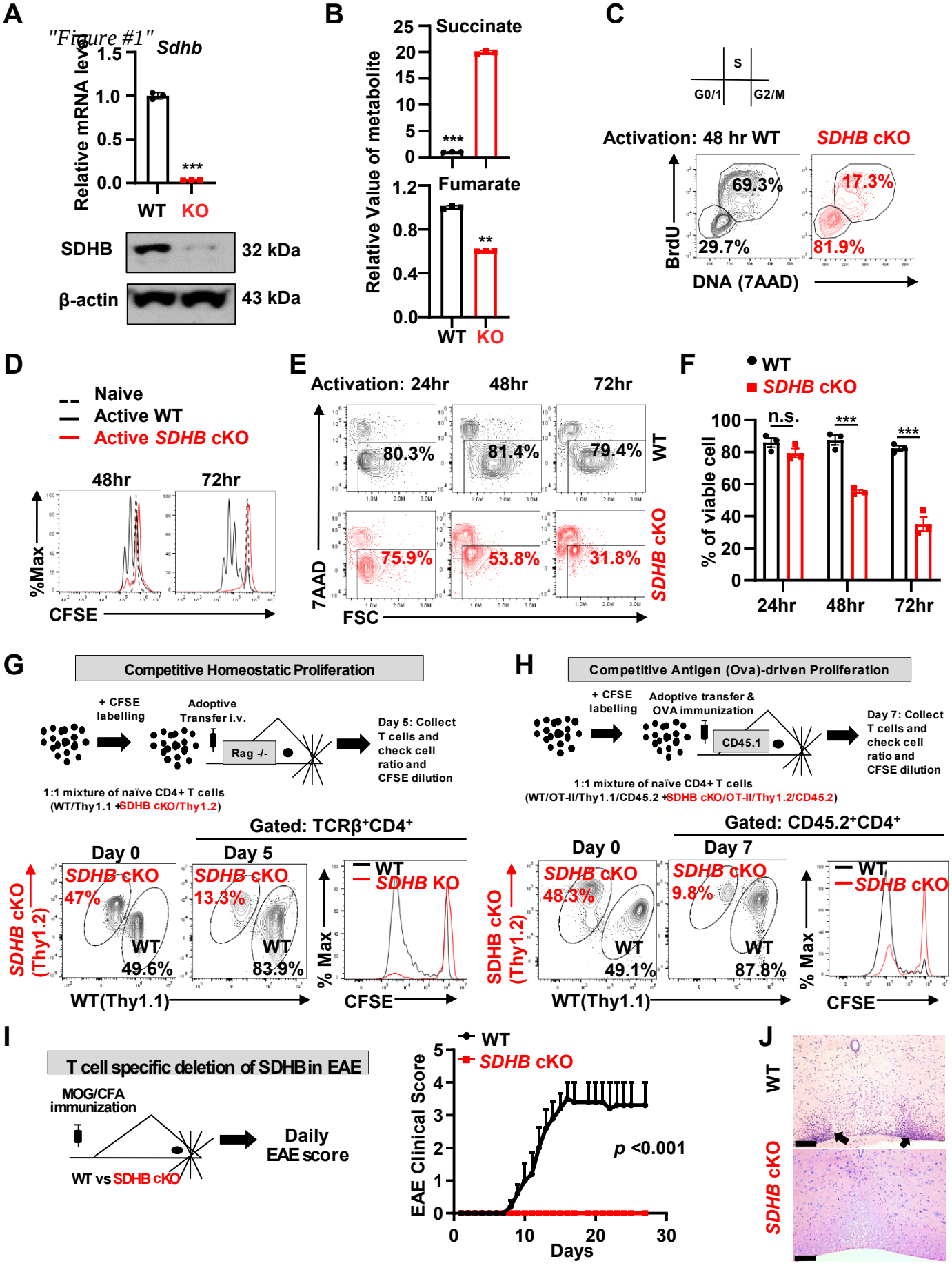

Figure 1. SDHB is required for T cell proliferation and survival.

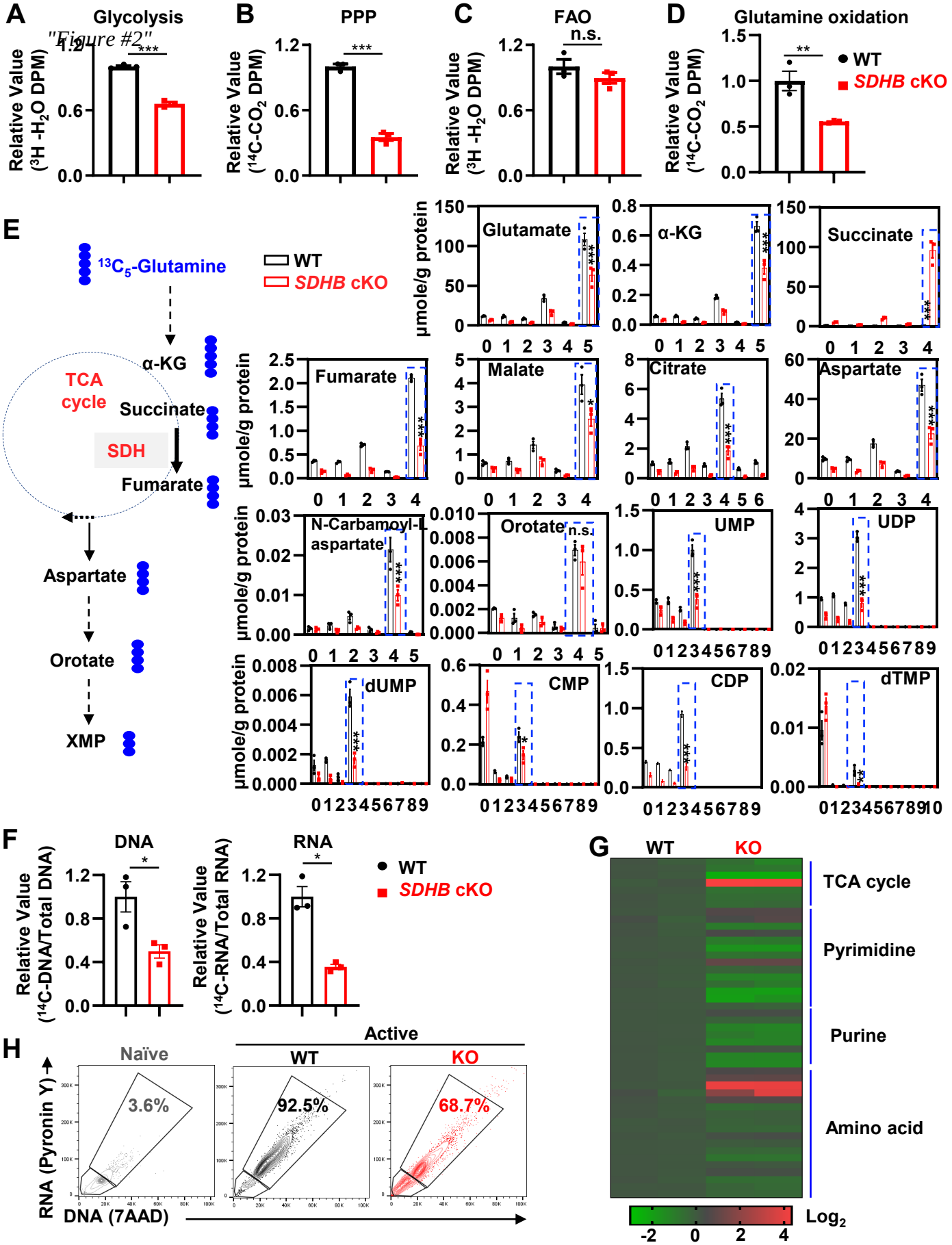

Figure 2. SDHB deficiency decouples the TCA cycle from nucleoside biosynthesis.

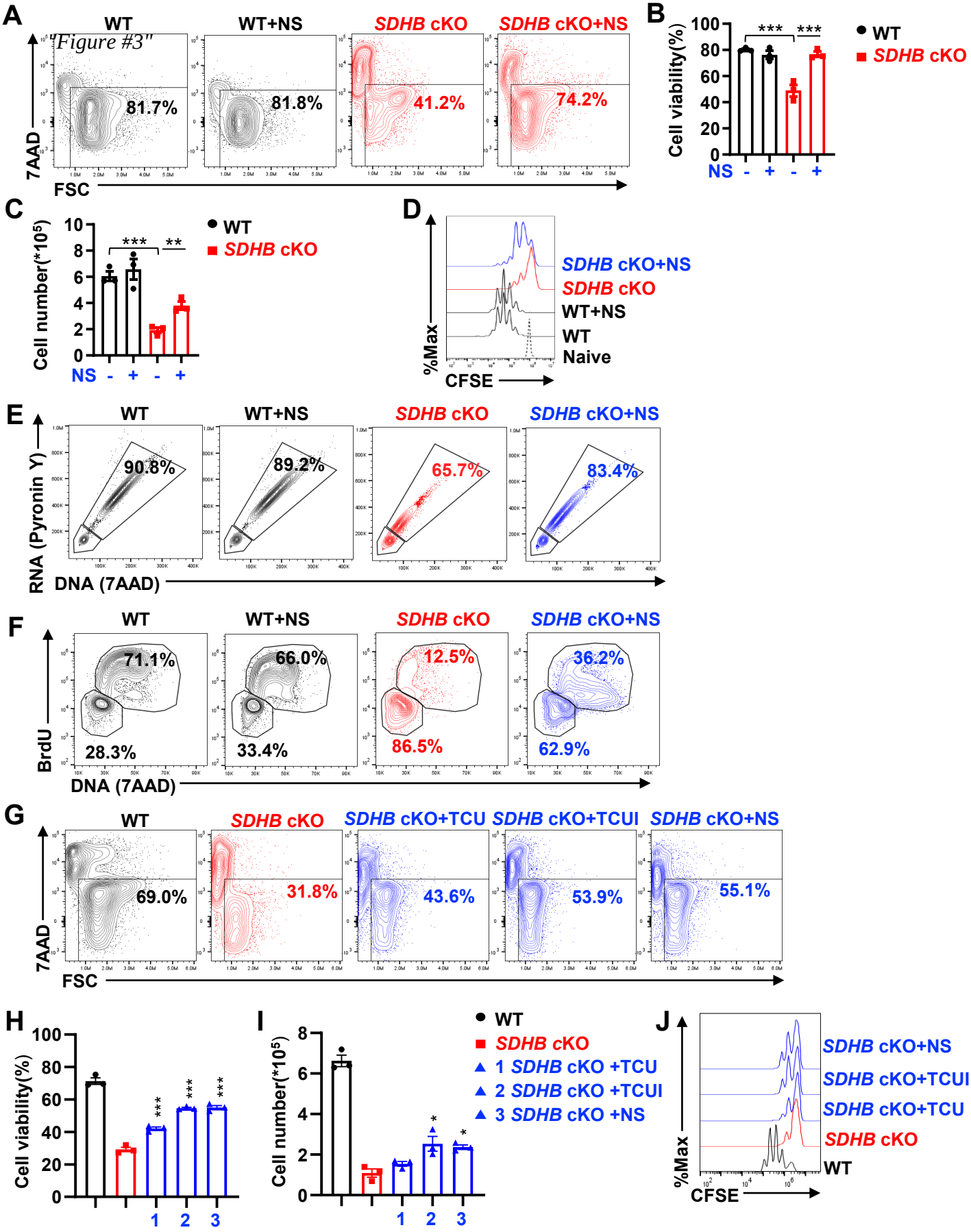

Figure 3. Nucleoside supplementation partially compensates for the loss of de novo biosynthesis of nucleotides in SDHB cKO T cells.

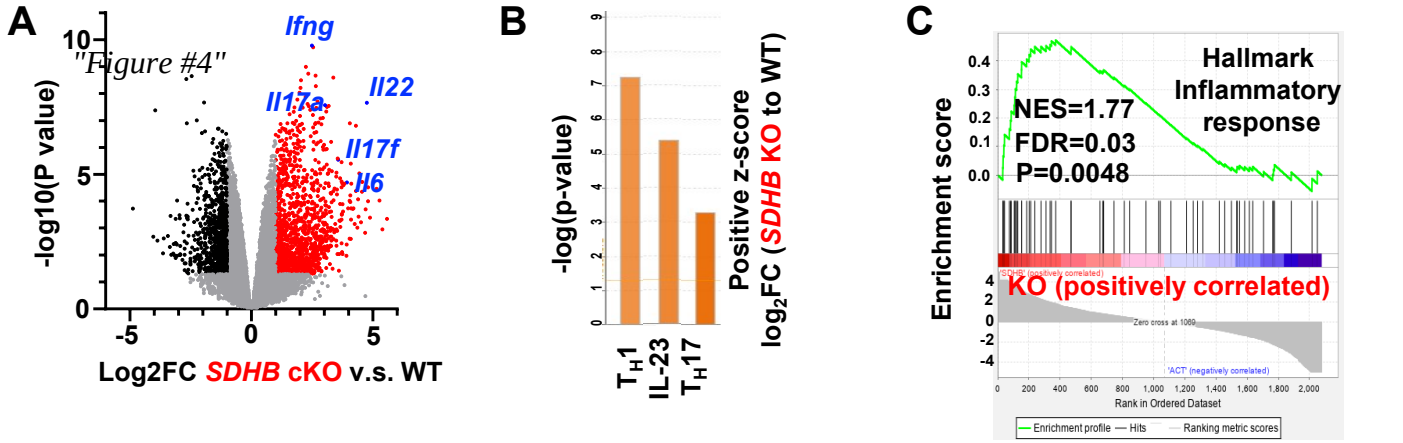

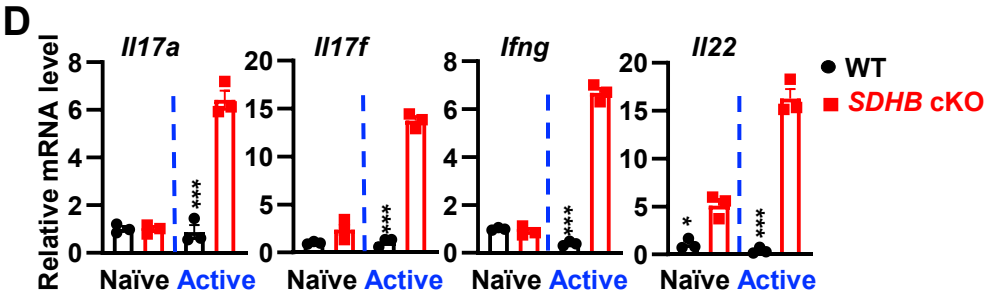

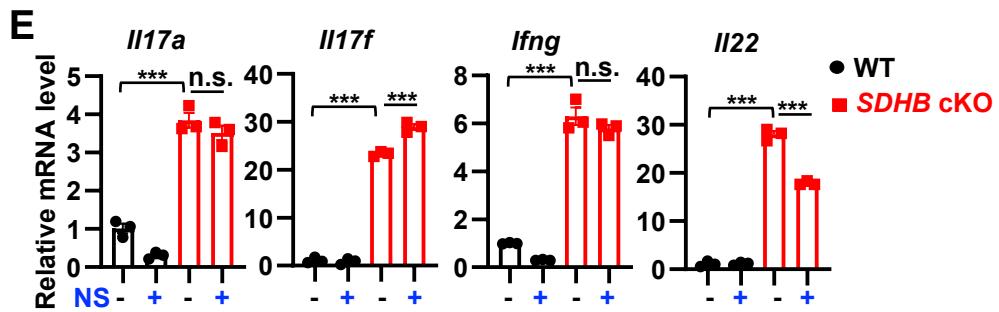

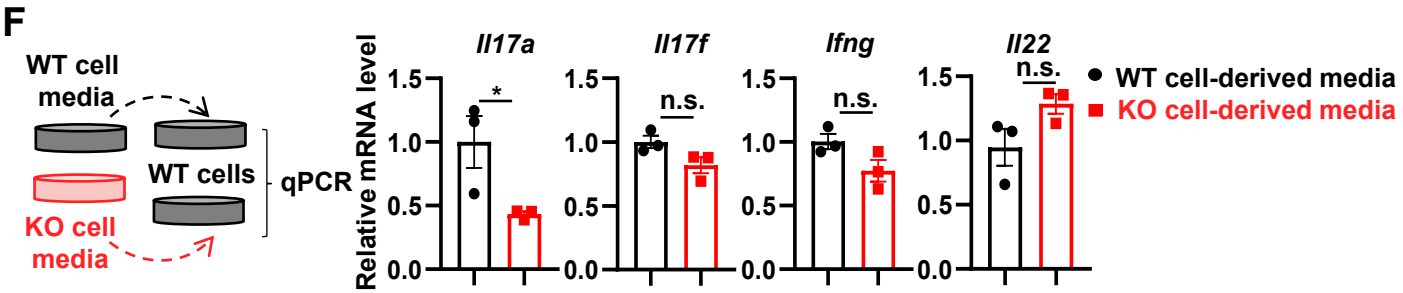

Figure 4. SDHB deficiency promotes a pro-inflammatory gene signature in T cells after activation.

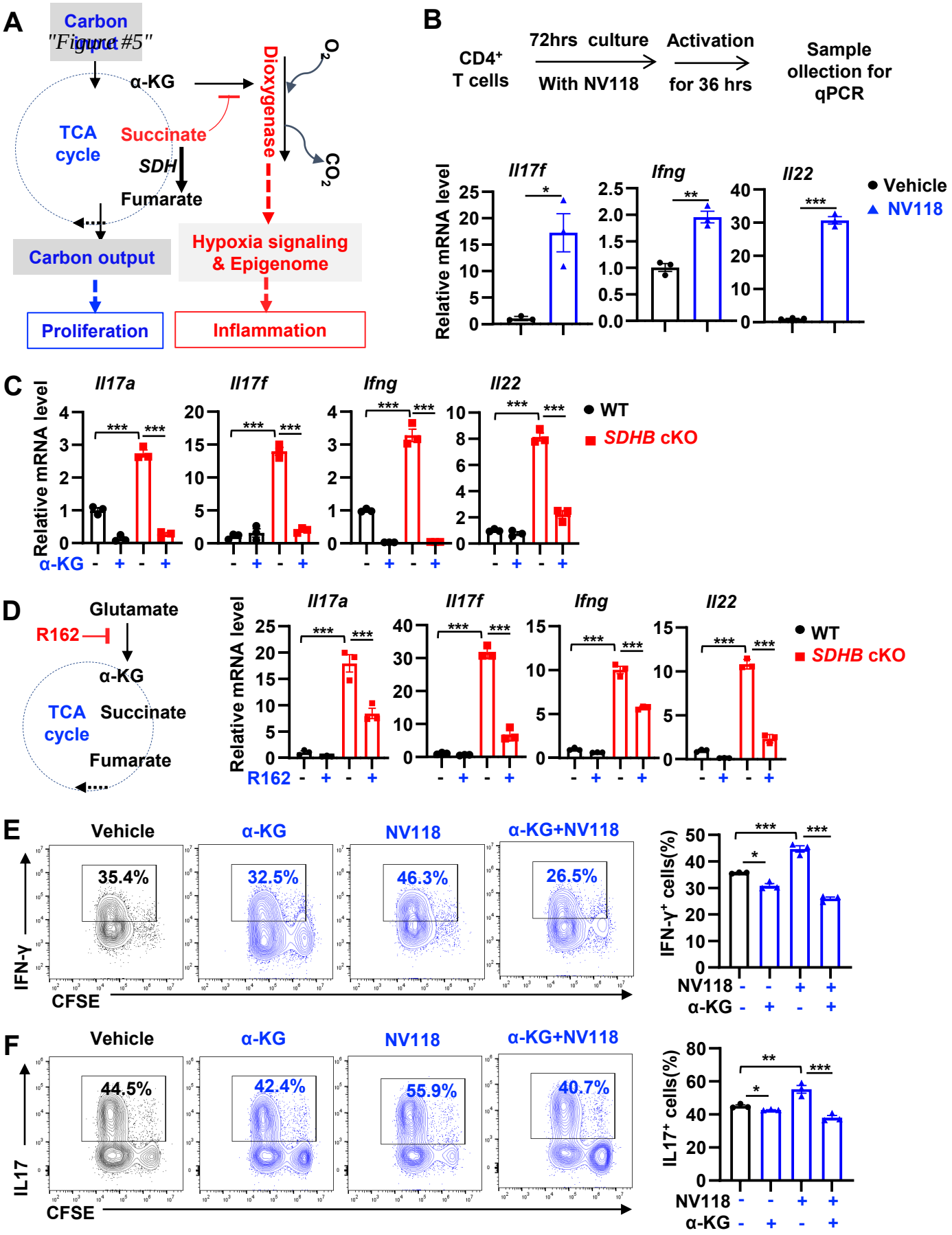

Figure 5. Increasing the succinate/α-KG ratio promotes pro-inflammatory signature in T cells after activation.

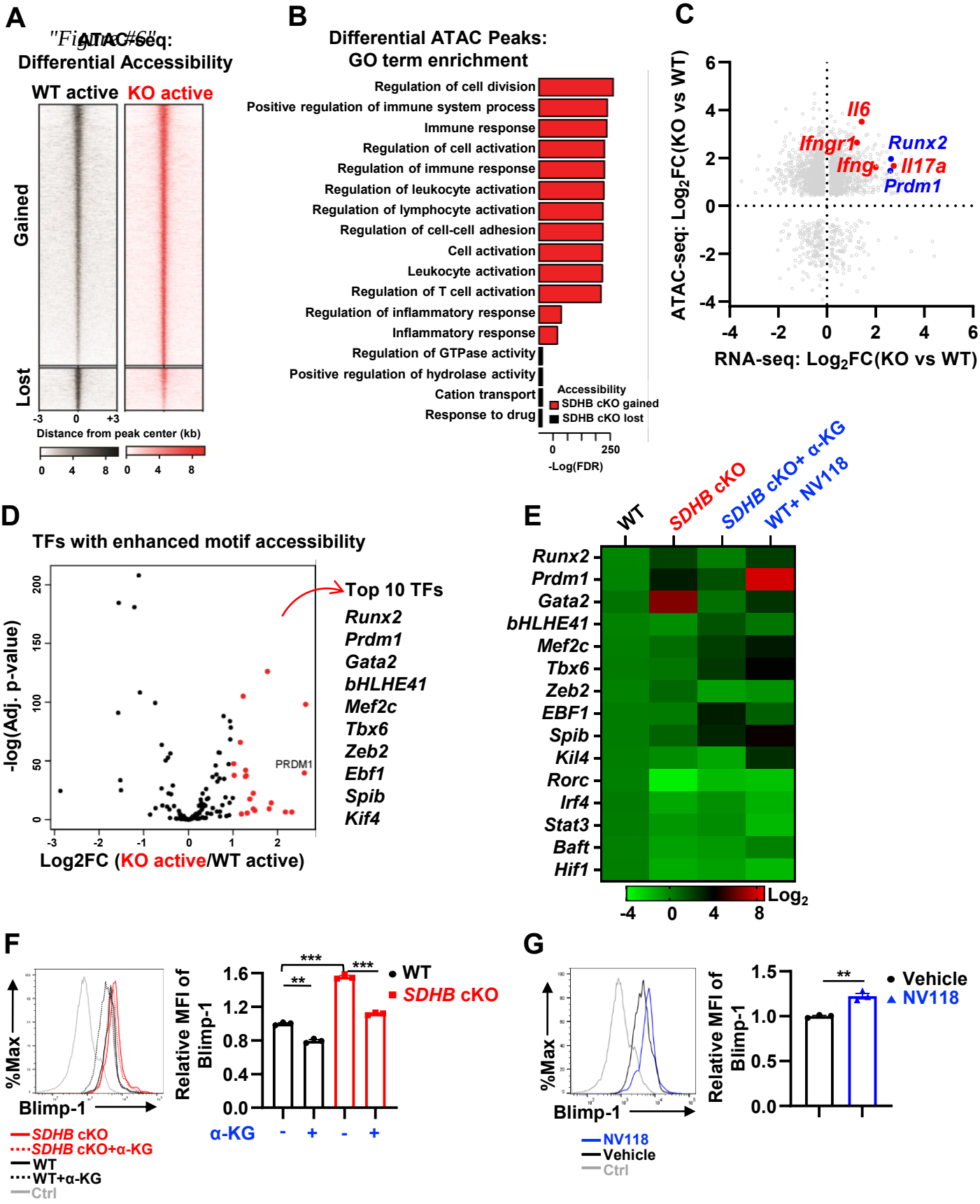

Figure 6. SDHB deficiency increases the level of succinate to enhance DNA accessibility and pro-inflammatory genes transcription.

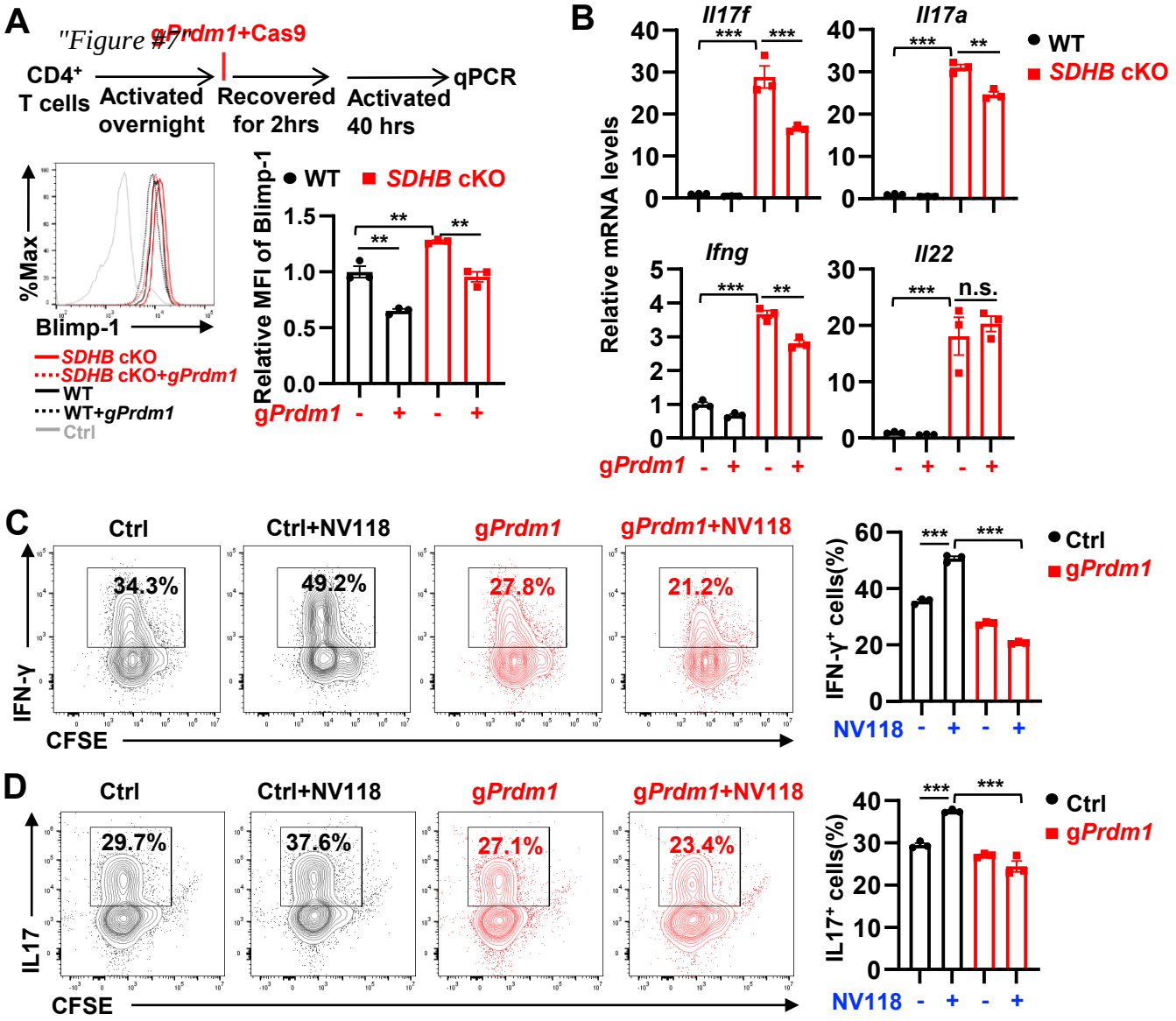

Figure 7. Succinate-mediated *Prdm1*/Blimp-1 expression contributes to proinflammatory signature in T cells.